UCSF
UC San Francisco Previously Published Works

Title
CD81 Controls Beige Fat Progenitor Cell Growth and Energy Balance via FAK Signaling

Permalink
https://escholarship.org/uc/item/1fb2d4gg

Journal
Cell, 182(3)

ISSN
0092-8674

Authors
Oguri, Yasuo
Shinoda, Kosaku
Kim, Hyeonwoo
et al.

Publication Date
2020-08-01

DOI
10.1016/j.cell.2020.06.021

Peer reviewed

eScholarship.org Powered by the California Digital Library
University of California

Cell

CD81 Controls Beige Fat Progenitor Cell Growth and Energy Balance via FAK Signaling

Graphical Abstract

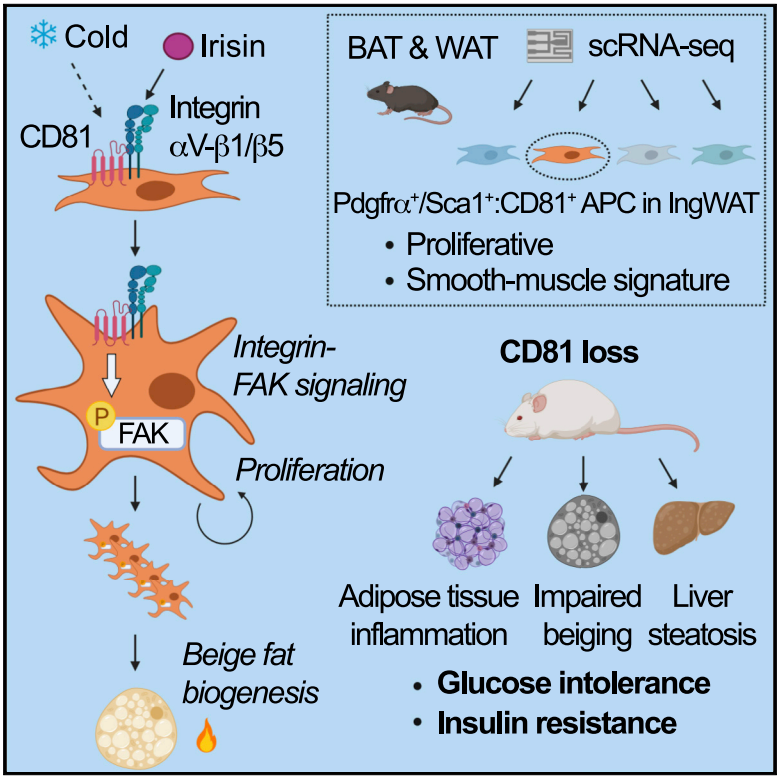

Highlights

- Beige fat progenitors are marked by cell surface proteins, PDGFRα, Sca1, and CD81
- Beige APC proliferation is regulated by temperature, genetic background, and aging
- CD81 mediates integrin-FAK signaling in response to irisin
- CD81 loss causes obesity, insulin resistance, and adipose tissue inflammation

Authors

Yasuo Oguri, Kosaku Shinoda, Hyeonwoo Kim, ..., Suneil K. Koliwad, Bruce M. Spiegelman, Shingo Kajimura

Correspondence

skajimur@bidmc.harvard.edu

In Brief

A subset of adipocyte progenitor cells give rise to beige fat through signaling responses to irisin through the action of specific integrins and the co-receptor CD81.

Oguri et al., 2020, Cell *182*, 1–15
August 6, 2020 © 2020 Elsevier Inc.
https://doi.org/10.1016/j.cell.2020.06.021

Please cite this article in press as: Oguri et al., CD81 Controls Beige Fat Progenitor Cell Growth and Energy Balance via FAK Signaling, Cell (2020), https://doi.org/10.1016/j.cell.2020.06.021

Cell

CellPress

Article

CD81 Controls Beige Fat Progenitor Cell Growth and Energy Balance via FAK Signaling

Yasuo Oguri,[1,2,3,4,13] Kosaku Shinoda,[1,2,3,5,13] Hyeonwoo Kim,[6,13] Diana L. Alba,[1,7,14] W. Reid Bolus,[1,7,14] Qiang Wang,[1,2,3,4] Zachary Brown,[1,2,3] Rachana N. Pradhan,[1,2,3] Kazuki Tajima,[1,2,3] Takeshi Yoneshiro,[1,2,3] Kenji Ikeda,[1,2,3,8] Yong Chen,[1,2,3,9] Rachel T. Cheang,[1,7] Kazuyuki Tsujino,[10] Caroline R. Kim,[6] Vanille Juliette Greiner,[1,11] Ritwik Datta,[12] Christopher D. Yang,[12] Kamran Atabai,[12] Michael T. McManus,[1,11] Suneil K. Koliwad,[1,7,15] Bruce M. Spiegelman,[6,15] and Shingo Kajimura[1,2,3,4,16,*]

[1]UCSF Diabetes Center, University of California, San Francisco, San Francisco, CA, USA
[2]Eli and Edythe Broad Center of Regeneration Medicine and Stem Cell Research, University of California, San Francisco, San Francisco, CA, USA
[3]Department of Cell and Tissue Biology, University of California, San Francisco, San Francisco, CA, USA
[4]Beth Israel Deaconess Medical Center, Division of Endocrinology, Diabetes & Metabolism, Harvard Medical School, Boston, MA, USA
[5]Department of Medicine and Molecular Pharmacology, Albert Einstein College of Medicine, New York, NY, USA
[6]Dana-Farber Cancer Institute, Harvard Medical School, Boston, MA, USA
[7]Department of Medicine, University of California, San Francisco, San Francisco, CA, USA
[8]Department of Molecular Endocrinology and Metabolism, Tokyo Medical and Dental University, Tokyo, Japan
[9]Department of Internal Medicine, Tongji Hospital, Tongji Medical College, Huazhong University of Science and Technology, Wuhan, China
[10]Department of Respiratory Medicine, National Hospital Organization Osaka Toneyama Medical Center, Osaka, Japan
[11]Department of Microbiology and Immunology, University of California, San Francisco, San Francisco, CA, USA
[12]Department of Medicine, Lung Biology Center, Cardiovascular Research Institute, University of California, San Francisco, San Francisco, CA, USA
[13]These authors contributed equally
[14]These authors contributed equally
[15]These authors contributed equally
[16]Lead Contact
*Correspondence: skajimur@bidmc.harvard.edu
https://doi.org/10.1016/j.cell.2020.06.021

SUMMARY

Adipose tissues dynamically remodel their cellular composition in response to external cues by stimulating beige adipocyte biogenesis; however, the developmental origin and pathways regulating this process remain insufficiently understood owing to adipose tissue heterogeneity. Here, we employed single-cell RNA-seq and identified a unique subset of adipocyte progenitor cells (APCs) that possessed the cell-intrinsic plasticity to give rise to beige fat. This beige APC population is proliferative and marked by cell-surface proteins, including PDGFRα, Sca1, and CD81. Notably, CD81 is not only a beige APC marker but also required for *de novo* beige fat biogenesis following cold exposure. CD81 forms a complex with αV/β1 and αV/β5 integrins and mediates the activation of integrin-FAK signaling in response to irisin. Importantly, CD81 loss causes diet-induced obesity, insulin resistance, and adipose tissue inflammation. These results suggest that CD81 functions as a key sensor of external inputs and controls beige APC proliferation and whole-body energy homeostasis.

INTRODUCTION

Adipose tissues comprise a dynamic metabolic organ that remodels the cellular size and composition in response to a variety of internal and external cues, including nutritional states and temperatures. Such metabolic adaptation that involves lipolysis, lipogenesis, adipogenesis, and thermogenesis, plays a central role in the regulation of energy homeostasis (Chouchani and Kajimura, 2019). A notable adaptive process within adipose tissues that has attracted particular attention is the "browning" or "beiging" of white adipose tissue (WAT), in which numerous mitochondria-enriched thermogenic adipocytes with multi-locular lipid droplets (a.k.a., beige adipocytes) emerge within WAT (Wu et al., 2012; Young et al., 1984). Importantly, adult humans possess beige fat: adult human brown adipose tissue (BAT) from the supraclavicular region contains mitochondria-enriched adipocytes that display a molecular signature resembling murine beige adipocytes (Lidell et al., 2013; Sharp et al., 2012; Shinoda et al., 2015a; Wu et al., 2012), and chronic cold acclimation or a β3-adrenergic receptor (β3-AR) agonist promotes the recruitment of new thermogenic fat (Finlin et al., 2018; van der Lans et al., 2013; Yoneshiro et al., 2013).

Please cite this article in press as: Oguri et al., CD81 Controls Beige Fat Progenitor Cell Growth and Energy Balance via FAK Signaling, Cell (2020), https://doi.org/10.1016/j.cell.2020.06.021

Emerging evidence suggests that increased beige fat biogenesis improves metabolic health in ways far beyond the induction of thermogenesis (Kajimura et al., 2015). For instance, selective activation of beige fat biogenesis improves systemic glucose tolerance and insulin sensitivity, reduces WAT inflammation and fibrosis, and protects against hepatic steatosis (Hasegawa et al., 2018; Ikeda et al., 2017; McDonald et al., 2015; Seale et al., 2011; Shinoda et al., 2015b). Conversely, impaired beige fat biogenesis results in insulin resistance, adipose tissue inflammation, fibrosis, and hepatic steatosis (Cohen et al., 2014; Wang et al., 2019). Thus, a better understanding of the regulatory circuits of beige fat biogenesis continues to be a significant area of research as it may lead to the development of therapeutic measures that improve metabolic health.

However, the developmental origins and regulation of beige fat are insufficiently understood. Lineage tracing analyses suggest that beige fat biogenesis involves both *de novo* differentiation from adipocyte progenitor cells (APCs) and reinstatement of thermogenic activity in mature white adipocytes (Shao et al., 2019). As for *de novo* beige adipogenesis, previous studies report that progenitors expressing *Acta2*, *Pax3*, *Pdgfra*, or *Pdgfrb* in the stromal vascular fraction (SVF) of WAT give rise to beige adipocytes following cold exposure (Berry et al., 2016; Lee et al., 2012; Sanchez-Gurmaches and Guertin, 2014; Vishvanath et al., 2016). Of note, PDGFRα and Sca1 are expressed on the cell surface of adipose stromal cells that differentiate into both beige and white adipocytes (Berry and Rodeheffer, 2013; Lee et al., 2012; Schulz et al., 2011); however, both markers are also expressed in other stromal populations in adipose tissues and many organs. For example, a subset of PDGFRα$^+$ cells in WAT expressing high levels of CD9 or ITGA5 are profibrogenic and drive adipose tissue fibrosis (Lin et al., 2018; Marcelin et al., 2017). Thus, it remains unclear what distinguishes beige APCs from other stromal cell types. Accordingly, this study employed single-cell RNA sequencing analysis (scRNA-seq) in order to identify beige APCs.

RESULTS

CD81 Is a Cell Surface Molecule for a Unique Subset of APCs

To characterize adipose stromal cells at single-cell resolution, we performed scRNA-seq analysis of lineage-negative (Lin$^-$) stromal cells from murine interscapular BAT (iBAT), inguinal WAT (Ing WAT), and epididymal WAT (Epi WAT) (Figures S1A–S1D). We employed the Fluidigm C1 system that allowed for deeper sequencing (~1–2 million reads/cell) despite fewer number of cells, as compared to the 10X Genomics platform that has been applied to adipose tissues (Burl et al., 2018; Hepler et al., 2018; Merrick et al., 2019; Schwalie et al., 2018). This scRNA-seq analysis identified at least five distinct clusters (types I–V) based on a t-distributed Stochastic Neighbor Embedding (t-SNE) map (Figure 1A). Among these groups, we found that stromal cells in the type III cluster expressed a number of genes (73.1% of the total type III-enriched genes) that were involved in vascular smooth muscle development and contraction (Figure 1B). For instance, violin plots showed that the type III cells expressed high levels of *Sm22* and *Acta2* (encoding alpha-smooth muscle actin [α-SMA]). Of note, most of these stromal cells, except type II cells, expressed high levels of *Pdgfra* (Figure 1C). Instead, the majority of type II cells expressed high levels of *Pdgfrb* and *Ednrb*, indicative of an endothelial signature (Hepler et al., 2018).

This "vascular smooth muscle" gene signature in type III cells caught our attention because stromal cells expressing *Acta2* or *Sm22* contribute to beige adipogenesis in Ing WAT (Berry et al., 2016; Long et al., 2014). To isolate live type III cells by fluorescence-activated cell sorting (FACS), we first searched for cell surface markers that were enriched in this cluster (Figure 1D). Among 370 known cell surface molecules, several candidates, including *Pdgfra*, *Ly6a* (coding Sca1), and *Cd81*, were highly expressed in type III cells relative to other groups (top 20 genes are listed in Table S1). Scatterplots from our scRNA-seq data showed that *Cd81* was expressed in a subset of APCs that express *Ly6a*/*Sca1* and *Pdgfra* (Figure 1E). A recent study reported that human CD34$^-$ APCs (Lin$^-$: CD29$^+$: CD34$^-$) differentiate to beige adipocytes expressing high levels of *Ucp1* and *Cited1* (Raajendiran et al., 2019). Indeed, 57% of the *Cd81*-expressing cells lacked *Cd34* expression. Moreover, we analyzed a recently published scRNA-seq dataset of mouse APCs (Hepler et al., 2018) and validated the existence of a stromal population expressing high levels of *Cd81*, *Sca1*, *Acta2*, and *Sm22* within this dataset (Figure S1E).

Accordingly, we aimed to isolate live type III cells by using antibodies against these cell-surface markers, followed by FACS. To establish the method, we first isolated Lin$^-$ stromal cells expressing α-SMA in Ing WAT by using *Acta2*-Cre^{ERT2}; *Rosa26*-LSL-tdTomato reporter mice that label all the α-SMA$^+$ cells following tamoxifen (Figure 1F). We found that CD81 protein expression was significantly higher in Lin$^-$: Sca1$^+$: tdTomato$^+$ (α-SMA$^+$) cells than other populations (Figure 1G, H). Conversely, isolated CD81$^+$ cells (Lin$^-$: Sca1$^+$: CD81$^+$) from Ing WAT-derived SVFs expressed significantly higher levels of the smooth muscle-related genes, including *Acta2*, *Sm22*, *Myl9*, and *Myh11*, relative to CD81$^-$ cells (Lin$^-$: Sca1$^+$: CD81$^-$) in Ing WAT (Figure 1I). Of note, the gene signature of isolated Lin$^-$ Sca1$^+$ CD81$^+$ cells from the Ing WAT resembled that of type III cells (Figure S1F), and PDGFRα and Sca1 marked nearly the same CD81$^+$ stromal population within the WAT of mice (Figure S1G). These data suggest that CD81 marks a subset of Sca1$^+$ PDGFRα$^+$ stromal cells possessing a smooth muscle-like signature and serves as a useful cell surface marker to isolate the type III cells from mouse WAT.

CD81$^+$ Stromal Cells Give Rise to Beige Adipocytes *In Vivo*

CD81, one of the tetraspanin family members, was originally identified as the target of an antiproliferative antibody for a human lymphoma cell line (Oren et al., 1990). To test if CD81 marks beige fat progenitors, we isolated CD81$^+$ and CD81$^-$ cells from the SVF of mouse Ing WAT by FACS (Figure 2A). After reaching confluency in culture, the sorted cells were differentiated under adipogenic conditions (Figure S2A). Oil-Red-O staining showed that CD81$^+$ cells differentiated into mature adipocytes, whereas CD81$^-$ cells showed limited adipogenic capacity even though they expressed Sca1 (Figure 2B). Differentiated CD81$^+$ cells

Please cite this article in press as: Oguri et al., CD81 Controls Beige Fat Progenitor Cell Growth and Energy Balance via FAK Signaling, Cell (2020), https://doi.org/10.1016/j.cell.2020.06.021

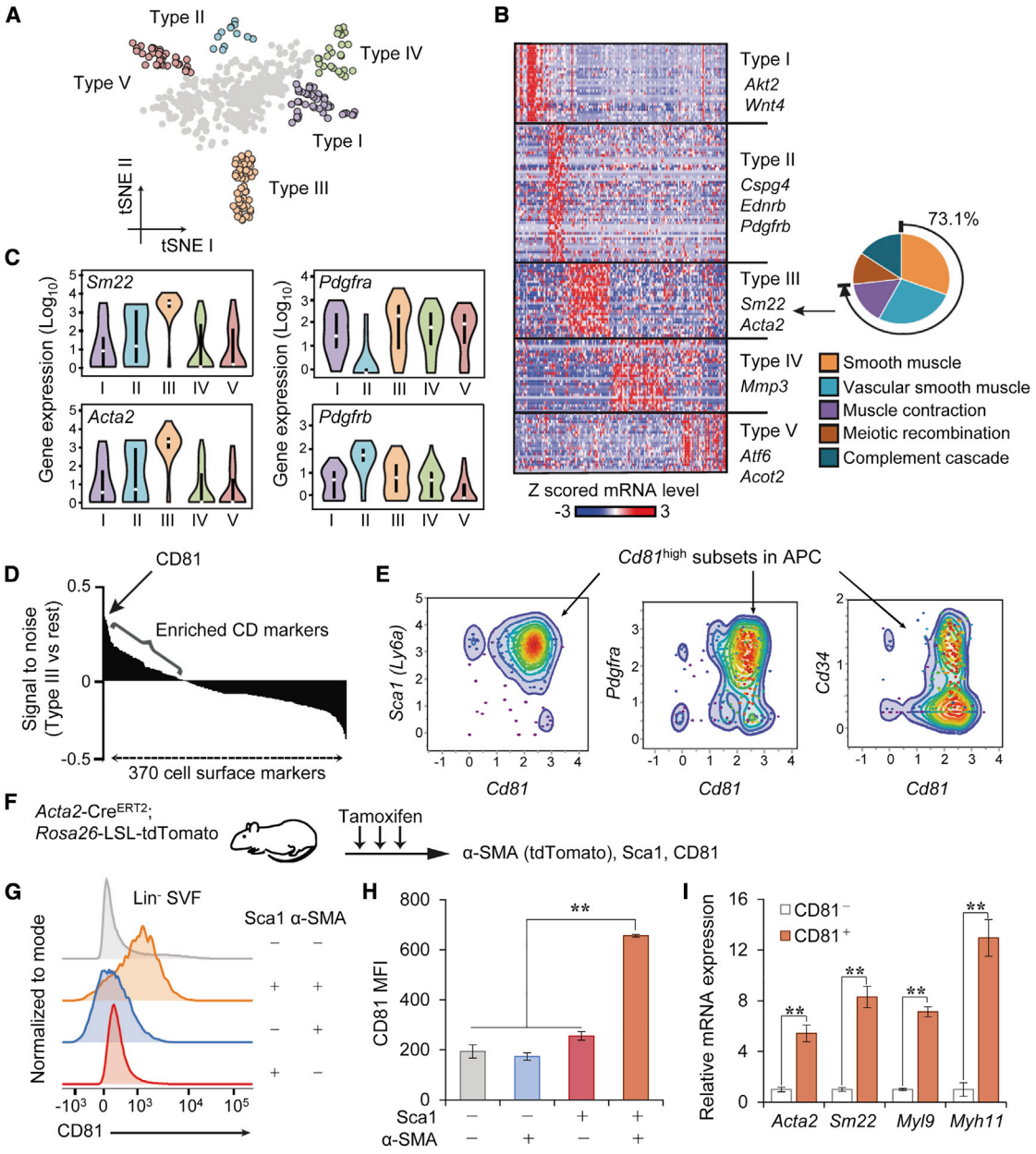

Figure 1. CD81 Marks a Subset of APCs

(A) Classification of Lin$^-$ stromal cells in mouse adipose tissues (type I–V clusters) on a t-SNE map.

(B) Heatmap of transcriptome in indicated cell clusters with representative genes. Right diagram: 73.1% of the type III cluster-enriched genes are involved in smooth muscle development and function.

(C) Violin plots showing mRNA levels of indicated genes in type I to V cell clusters.

(D) Expression of cell surface genes, including CD81, that are enriched in type III cluster.

(E) Scatterplots showing the distribution of *Cd81*$^+$ cells in *Sca1*$^+$, *Pdgfra*$^+$, or *Cd34*$^+$ cells.

(F) Illustration of the experiments in (G) and (H).

(G) Distribution of CD81$^+$ cells among Lin$^-$: Sca1$^+$: tdTomato$^+$ cells from the Ing WAT of *Acta2* reporter mice. n = 3.

(H) CD81 expression (mean fluorescence intensity [MFI]) in indicated cells from mice in (G). **p < 0.01 by one-way ANOVA followed by Bonferroni's post hoc test.

(I) mRNA expression of smooth muscle-enriched genes in indicated cells from Ing WAT. CD81$^-$ cells, n = 6; CD81$^+$ cells, n = 4. **p < 0.01 by unpaired Student's t test.

Data in (H) and (I) are represented as mean ± SEM.

Please cite this article in press as: Oguri et al., CD81 Controls Beige Fat Progenitor Cell Growth and Energy Balance via FAK Signaling, Cell (2020), https://doi.org/10.1016/j.cell.2020.06.021

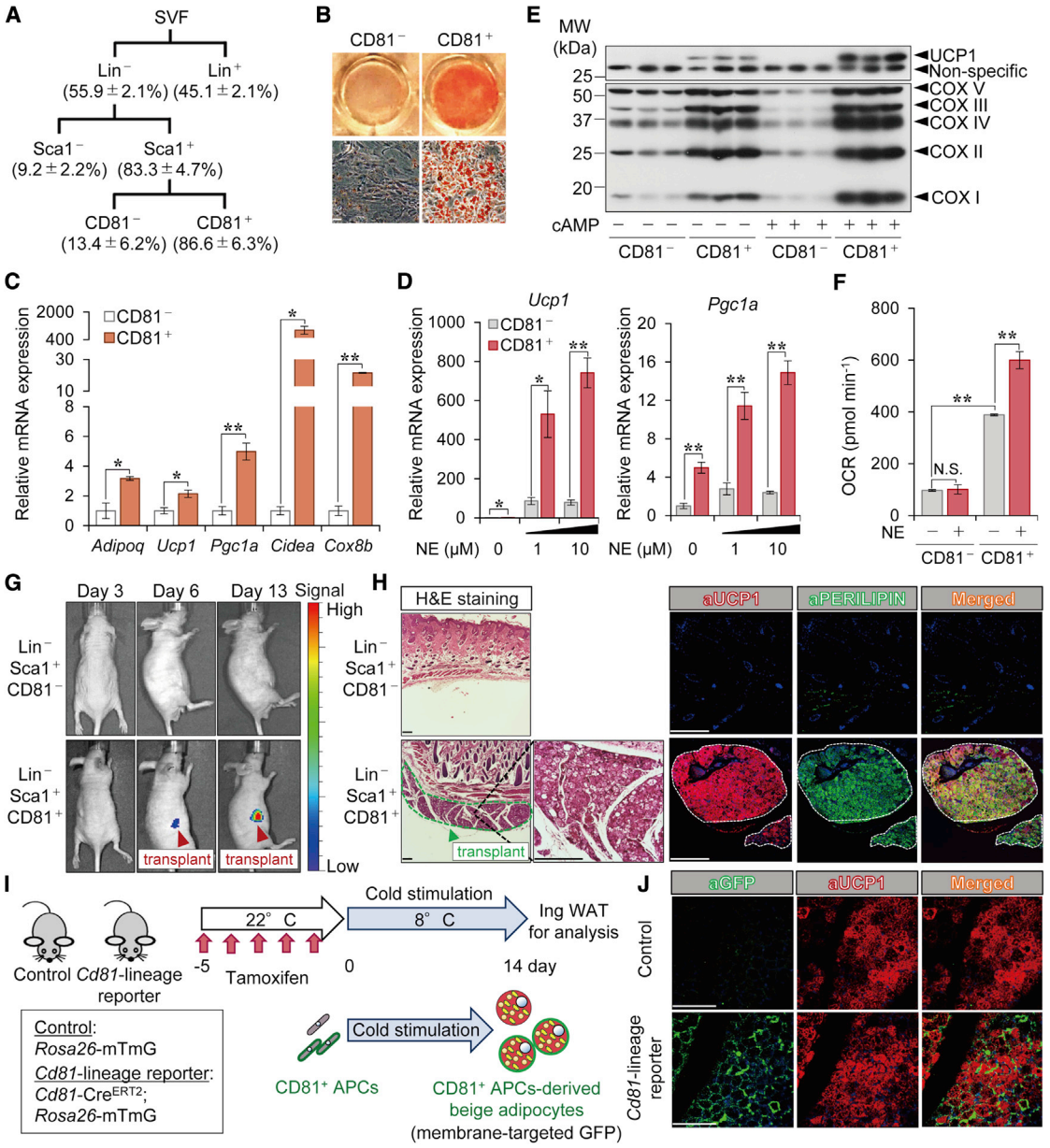

Figure 2. CD81⁺ Stromal Cells Give Rise to Beige Adipocytes

(A) The scheme for the FACS analysis to isolate indicated cells from mouse inguinal WAT. The percentage yield of each population is based on the Ing WAT-derived SVFs after overnight culture. n = 4.

(B) Oil-Red-O staining of differentiated CD81⁻ and CD81⁺ cells. Cells from the Ing WAT of BL6 mice were differentiated for 6 days under an adipogenic condition. Low (top) and high magnification (bottom) are shown. Scale bars, 50 μm.

(C) mRNA expression of indicated genes in differentiated cells in (B). n = 3.

(D) mRNA expression of *Ucp1* and *Pgc1a* in differentiated cells stimulated with or without NE for 4 h. (C and D) *p < 0.05, **p < 0.01 by unpaired Student's t test.

(E) Immunoblotting for UCP1 and indicated mitochondrial proteins in differentiated cells stimulated with or without forskolin (cAMP, 10 μM) for 6 h.

(F) OCR (pmol min^{-1}) in differentiated cells treated with or without NE (10 μM). n = 10. **p < 0.01 by one-way ANOVA followed by Bonferroni's post hoc test.

(G) Luciferase activity of transplants at indicated days after transplantation. Arrowhead indicates luciferase⁺ (UCP1⁺) transplants.

(H) H&E staining and immunofluorescent staining for UCP1 and PERILIPIN in the transplants in (G). DAPI for counterstaining of immunofluorescent staining. Scale bars, 200 μm.

(I) Illustration of the experiments in *Cd81*-lineage reporter mice.

(J) Immunofluorescent staining for GFP and UCP1 in the Ing WAT from indicated mice. Scale bars, 100 μm.

Data in (A) (C), (D), and (F) are represented as mean ± SEM.

Please cite this article in press as: Oguri et al., CD81 Controls Beige Fat Progenitor Cell Growth and Energy Balance via FAK Signaling, Cell (2020), https://doi.org/10.1016/j.cell.2020.06.021

expressed many brown/beige fat-selective genes, such as *Ucp1*, *Pgc1a*, *Cidea*, and *Cox8b* (Figure 2C). Moreover, differentiated CD81$^+$ cells expressed significantly higher mRNA levels of *Ucp1* and *Pgc1a* relative to CD81$^-$ cells, particularly after the cells were stimulated with norepinephrine (NE) (Figure 2D). It is worth noting that CD81$^+$ cells possessed a cell-intrinsic capacity for beige adipogenesis without the browning cues (PPARγ agonists or NE): differentiated CD81$^+$ cells expressed high levels of *Ucp1*, *Pgc1a*, *Cidea*, and *Cox8b*, even under the culture condition without rosiglitazone during the adipogenic induction phase (Figures S2B and S2C). Furthermore, differentiated CD81$^+$ cells expressed higher protein levels of UCP1 and members of the mitochondrial OXPHOS complex than did CD81$^-$ cells, both in the presence and absence of forskolin (cyclic AMP [cAMP]) (Figure 2E). Importantly, CD81$^+$-derived differentiated adipocytes responded to NE by increasing both their total and uncoupled oxygen consumption rate (OCR), whereas CD81$^-$ cells did not have such responsiveness to NE (Figures 2F and S2D).

To determine if CD81$^+$ cells give rise to beige fat *in vivo*, we isolated CD81$^+$ cells and CD81$^-$ cells from the Ing WAT of UCP1-luciferase mice (*ThermoMouse*) in which luciferase activity reflects UCP1 expression (Galmozzi et al., 2014). Isolated cells were mixed in HydroMatrix gel and then transplanted into the subcutaneous region of immunodeficient *Nude* mice (Figures S2E and S2F). At 6 days after transplantation, we detected luciferase activity (i.e., UCP1 expression) in CD81$^+$ cell transplants, but not in CD81$^-$ cell transplants (Figure 2G). The luciferase activity of CD81$^+$ cell transplants was further increased 13 days after transplantation. Additionally, the CD81$^+$ cell transplants derived from *ThermoMouse* contained multilocular adipocytes and expressed endogenous UCP1 and PERILIPIN (Figures 2H and S2G). We also found that the CD81$^+$ cell transplants expressed many thermogenic fat-selective genes at high levels similar to what is seen in cold-induced beige fat (Figure S2H). By contrast, CD81$^-$ transplants did not form visible fat tissues.

Next, we used lineage tracing of CD81$^+$ cells within the adipose tissue to further determine the extent to which these cells differentiate into beige fat *in vivo*. To this end, we generated inducible *Cd81*-Cre^{ERT2} mice (knockin mice that carry Cre^{ERT2} in the *Cd81* gene locus at the N terminus) and crossed them with *Rosa26*-mTmG reporter mice. Following pre-treatment with tamoxifen at ambient temperature for 5 consecutive days, the *Cd81*-lineage reporter mice (*Cd81*-Cre^{ERT2}; *Rosa26*-mTmG) and control mice (*Rosa26*-mTmG mice) were acclimated to 8°C for 14 days to induce beige fat biogenesis (Figure 2I). Following cold exposure, a large number of cold-induced UCP1$^+$ beige adipocytes in the Ing WAT were derived from CD81$^+$ cells (Figures 2J and S2I). Of note, some UCP1$^+$ beige adipocytes in the Ing WAT of *Cd81*-lineage reporter mice did not express GFP (Figure S2J), consistent with works suggesting that some beige adipocytes are derived from mature adipocytes or other developmental lineages (Shao et al., 2019). On the other hand, the iBAT contained a very small fraction of GFP$^+$ UCP1$^+$ brown adipocytes after cold acclimation (Figure S2K), suggesting that CD81$^+$ cells in iBAT are distinct from *Myf5*$^+$ brown progenitors. In addition, CD81$^+$-derived cells were distinct from PDGFRα^+ fibroblasts in Ing WAT after cold acclimation (Figure S2L), reinforcing the results that CD81 marks a subset of PDGFRα^+ stromal cells in the adipose tissue. Together, these data suggest that CD81 marks an APC population that possesses the cell-intrinsic plasticity to give rise to beige adipocytes. Thus, we termed this population as beige APCs.

CD81$^+$ APCs Is a Proliferative Population in the Inguinal WAT

CD81 protein is expressed highly in adipose tissues and smooth muscle, and also expressed in other tissues at lower levels. Hence, we probed CD81$^+$ APCs in the Ing WAT for any functionally unique properties. To this end, we isolated CD81$^+$ and CD81$^-$ cells from iBAT, Ing WAT, and Epi WAT of wild-type mice under the ambient temperature condition, and analyzed their transcriptome by RNA-seq (Figure 3A). Hierarchical clustering revealed that CD81$^+$ APCs exhibited a distinct molecular signature from CD81$^-$ cells in Ing WAT and other populations in the iBAT and Epi WAT (Figure 3B). Gene Ontology (GO) analysis of the transcriptome data suggested that biological pathways relating to cell growth, actin filament processes, apoptotic signaling, cell cycle, and wound healing, were significantly upregulated in the Ing WAT-derived CD81$^+$ cells (Figure 3C). These pathways were unique to Ing WAT-derived CD81$^+$ cells because GO analysis of the transcriptome in CD81$^+$ cells from the Epi WAT or iBAT did not highlight these biological pathways (Figure S3A). Consistent with the pathway analysis, we found a significantly more Ki67$^+$ cells among Ing WAT-derived CD81$^+$ cells than among Ing WAT-derived CD81$^-$ cells (Figure 3D). Furthermore, isolated Ing WAT-derived CD81$^+$ cells grew significantly faster than did either their CD81$^-$ counterparts or CD81$^+$ APCs from Epi WAT (Figures 3E and 3F).

To ask how Ing WAT-derived CD81$^+$ APC proliferation is regulated by cold exposure and genetic factors, we isolated CD81$^+$ cells from the Ing WAT of wild-type C57BL/6J mice that were exposed to 4°C for 4 days or 22°C before receiving an intraperitoneal injection of 5-ethynyl-2′-deoxyuridine (EdU) (Figure 3G). Following the EdU pulse, we detected a robust EdU incorporation in Ing WAT-derived CD81$^+$ APCs, and this was further increased by cold exposure (Figure 3H). Next, we examined the impact of genetic background and age on the proliferation of CD81$^+$ APCs, because 129SVE mice possess higher amounts of beige adipocytes and are more resistant to diet-induced obesity than C57BL/6J mice (Guerra et al., 1998), while aging negatively impacts beige fat biogenesis (Berry et al., 2017; Tajima et al., 2019). We found that the proliferative rate of CD81$^+$ APCs from the Ing WAT of 129SVE mice was significantly higher than corresponding APCs from C57BL/6J mice, although CD81$^+$ cells grew faster than CD81$^-$ cells regardless of the genetic background (Figure 3I). Additionally, the cell growth rate of Ing WAT-derived CD81$^+$ APCs was significantly attenuated in 60-week-old mice, in which cold-induced beige fat biogenesis was also impaired (Figures 3J and S3B). We also found that these 60-week-old mice had fewer CD81$^+$ APCs in the Ing WAT relative to young mice (8- to 10-week-old) (Figure S3C). The data are aligned with the CD81$^+$ APC transcriptomics data, because the cellular senescence pathway, often upregulated by aging, was repressed in CD81$^+$ APCs from young mice (Figure S3D). These results suggest that CD81$^+$ APCs in Ing WAT is unique among other stromal cells in the high

Please cite this article in press as: Oguri et al., CD81 Controls Beige Fat Progenitor Cell Growth and Energy Balance via FAK Signaling, Cell (2020), https://doi.org/10.1016/j.cell.2020.06.021

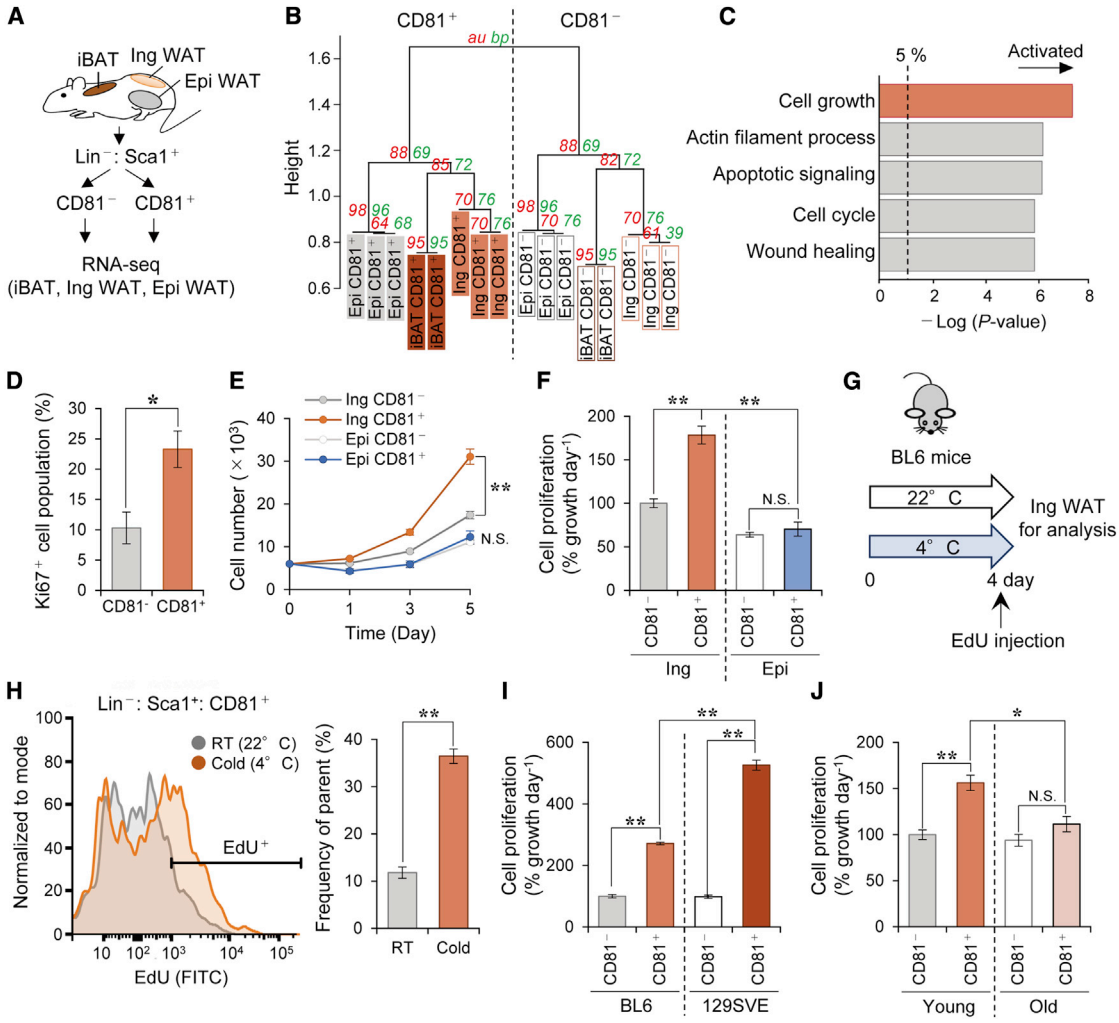

Figure 3. CD81⁺ APCs in the Inguinal WAT Is a Proliferative Stromal Population

(A) Schematic illustration of the experiment. CD81⁺ cells (Lin⁻: Sca1⁺: CD81⁺) and CD81⁻ cells (Lin⁻: Sca1⁺: CD81⁻) were isolated from indicated fat depots of 10-week-old BL6 mice.

(B) Hierarchical clustering of transcriptomics. The horizontal distance represents similarities among each cluster as visualized by pvclust in R. Approximately unbiased (*au*; red) p value and bootstrap probability (*bp*; green) values as measures of certainty for clusters.

(C) Upregulated biological pathways in CD81⁺ cells relative to CD81⁻ cells from Ing WAT. n = 3.

(D) Ki67⁺ cell population (%) in CD81⁻ and CD81⁺ cells from Ing WAT of BL6 mice. n = 5. *p < 0.05 by unpaired Student's t test.

(E) Cell number at indicated time points after seeding cells on non-coated culture plates. Cells were isolated from Ing WAT or Epi WAT of BL6 mice. n = 4. **p < 0.01 by two-way repeated-measures ANOVA.

(F) Cell proliferation rate (% growth day^{-1}) of indicated cells in (E). Data were presented as relative values to the growth rate of CD81⁻ cell in Ing WAT.

(G) Illustration of the experiments in (H).

(H) EdU incorporation in CD81⁺ cells in (G). Right panel shows quantification of EdU⁺ cells. n = 3. **p < 0.01 by unpaired Student's t test.

(I) Cell proliferation rate of indicated cells from Ing WAT of BL6 and 129SVE male mice (12-week-old). n = 4.

(J) Cell proliferation rate of indicated cells from Ing WAT of young (8–10 weeks) and old (60 weeks) male BL6 mice. Young, n = 10; old, n = 5. (F), (I), and (J) *p < 0.05, **p < 0.01 by one-way ANOVA followed by Bonferroni's post hoc test.

Data in (D)–(F) and (H)–(J) are represented as mean ± SEM.

proliferative capacity, which is regulated by cold exposure, genetic background, and aging.

CD81 Mediates Irisin-Induced FAK Signaling by Forming Complexes with αV/β1 and αV/β5 Integrins

To determine the mechanisms underlying the highly proliferative nature of CD81⁺ APCs in the Ing WAT, we next ran a functional enrichment analysis on the transcriptome data. The analysis showed that the focal adhesion pathway, including the focal adhesion kinase (FAK: coded by the *Ptk2* gene), was upregulated in Ing WAT-derived CD81⁺ APCs relative to CD81⁻ cells (Figures 4A and S4A). Thus, we examined the extent to which FAK controls Ing WAT-derived CD81⁺ APC proliferation by genetic and pharmacological approaches. We found that *Ptk2*

Please cite this article in press as: Oguri et al., CD81 Controls Beige Fat Progenitor Cell Growth and Energy Balance via FAK Signaling, Cell (2020), https://doi.org/10.1016/j.cell.2020.06.021

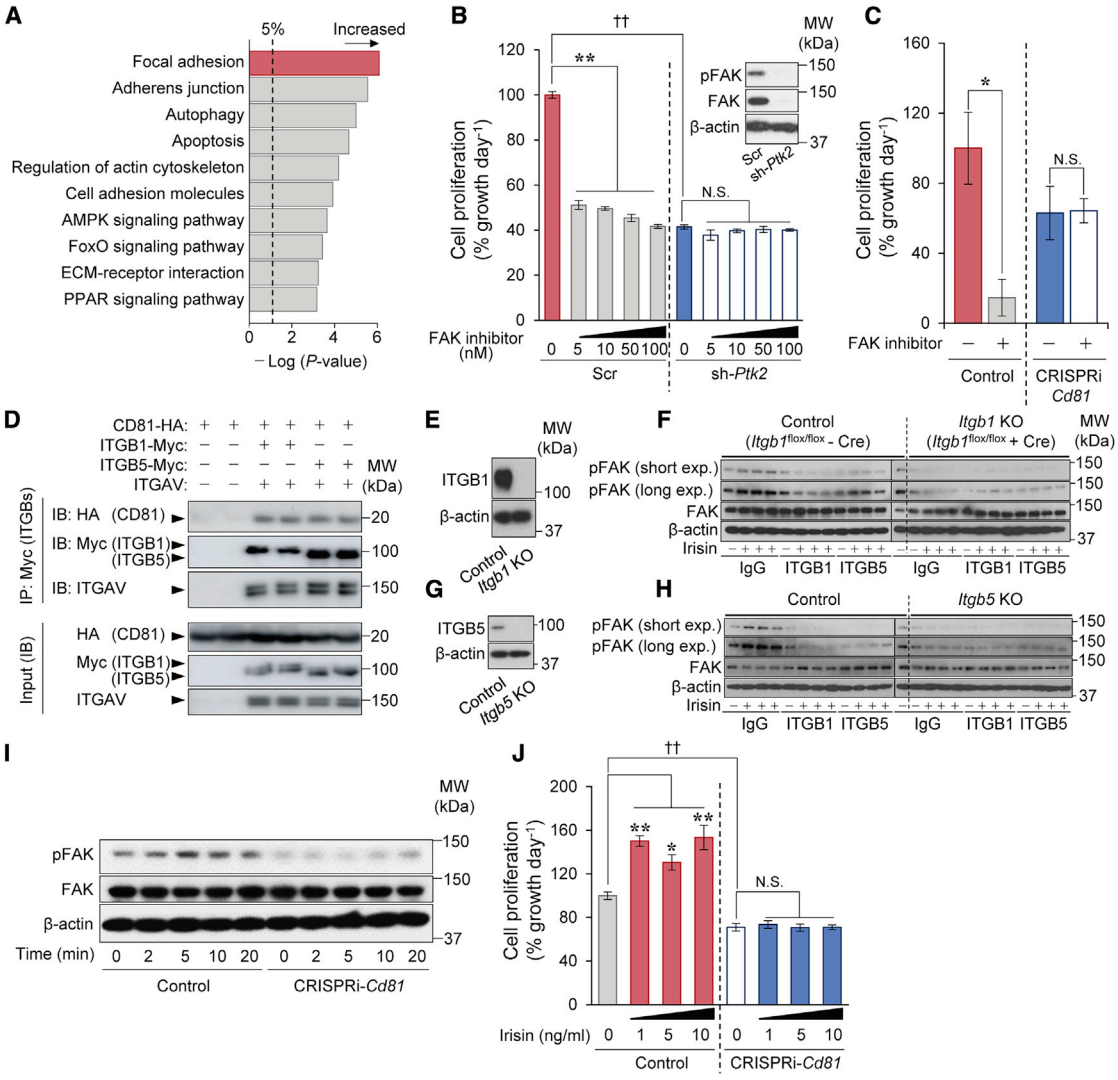

Figure 4. CD81 Forms Complexes with αV/β1 and αV/β5 Integrins and Mediates Irisin-Induced FAK Signaling

(A) The upregulated KEGG signaling pathways in CD81$^+$ cells relative to CD81$^-$ cells from Ing WAT. n = 3.

(B) The effect of FAK inhibitor (PF-573228) on cell proliferation rate of CD81$^+$ cells expressing shRNA targeting FAK (sh-*Ptk2*) or a scrambled control (Scr). Cells were treated with PF-573228 or vehicle (DMSO) for 4 days. n = 4. Inset: immunoblotting for FAK and β-actin.

(C) The effect of PF-573228 at 1 μM on cell proliferation rate of Lin$^-$: Sca1$^+$ stromal cells from CRISPRi-*Cd81* mice and littermate controls. n = 3. *p < 0.05 by unpaired Student's t test.

(D) Immunoblotting for indicated proteins in HEK293T cells. Cell lysates were immunoprecipitated with Myc-tag beads (ITGB1 and ITGB5) and detected by antibodies against HA (CD81), Myc (ITGB1, ITGB5), and ITGAV. Inputs were shown in lower panels. The pellet and input were loaded at a ratio of 20:1.

(E) Immunoblotting for ITGB1 and β-actin in control and *Itgb1* KO CD81$^+$ cells from the Ing WAT of *Itgb1*$^{flox/flox}$ mice.

(F) Immunoblotting for FAK phosphorylation (pTyr397) (short and long exposure), total FAK, and β-actin in cells in (E) following irisin treatment. Cell lysates from control cells without irisin were included in the leftmost lane of the right panel (*Itgb1* KO cells) as a reference.

(G) Immunoblotting for ITGB5 and β-actin in CD81$^+$ cells from the Ing WAT of *Itgb5* KO or control mice.

(H) Immunoblotting for indicated proteins in cells in (G) following irisin treatment.

(I) Immunoblotting for indicated proteins in Lin$^-$: Sca1$^+$ stromal cells from the Ing WAT of CRISPRi-*Cd81* mice and controls. Time point 0 is the cells prior to irisin treatment (control).

(J) Cell proliferation rate of Lin$^-$: Sca1$^+$ cells in (I). Isolated cells were treated with irisin at indicated doses for 5 days. n = 4. (B and J) *p < 0.05, **p < 0.01 by one-way ANOVA followed by Dunnett's post hoc test. ††p < 0.01 by unpaired Student's t test with Bonferroni's correction.

Data in (B), (C), and (J) are represented as mean ± SEM.

knockdown by lentiviral short hairpin RNA (shRNA) significantly inhibited cell proliferation in CD81$^+$ cells. Furthermore, inhibition of FAK by PF-573228, a specific ATP-competitive inhibitor of FAK, potently reduced CD81$^+$ APC proliferation over a wide concentration range, whereas this reduction was not seen when FAK was depleted in the cells (Figures 4B and S4B). To test if CD81 is

Please cite this article in press as: Oguri et al., CD81 Controls Beige Fat Progenitor Cell Growth and Energy Balance via FAK Signaling, Cell (2020), https://doi.org/10.1016/j.cell.2020.06.021

required for FAK signaling, we next depleted *Cd81* by CRISPRi in which catalytically inactive Cas9 protein (dCas9) is fused to a Krüppel-associated box (KRAB) domain. Transgenic mice expressing a gRNA targeting *Cd81* were crossed with dCas9-KRAB mice to generate *Cd81*-deficient mice (CRISPRi-*Cd81* mice) (Figures S4C–S4E). We found that the proliferation of Lin^- $Sca1^+$ stromal cells in the Ing WAT of CRISPRi-*Cd81* mice was significantly lower than corresponding cells from control mice regardless of the culture conditions (plate-coating, FBS concentrations) (Figures S4F and S4G), while PF-573228 treatment did not diminish the proliferative rate of CD81-deficient cells (Figure 4C). These results indicate that FAK signaling is required for the proliferation of $CD81^+$ APCs in Ing WAT and also suggest that rather than merely serving as a surface marker, CD81 is a functional regulator of beige APC proliferation.

CD81 is known to interact with integrins (Berditchevski et al., 1996; Termini and Gillette, 2017). Notably, *Itgav* (integrin αV, a.k.a., CD51) was dominantly expressed in $CD81^+$ APCs from the Ing WAT at a significantly higher level than $CD81^-$ APCs (Figure S5A). Among integrin β chains (ITGB), $CD81^+$ cells expressed *Itgb1* at the highest level, followed by *Itgb5*. This result caught our particular attention because a recent study showed that irisin, an exercise-induced myokine that promotes beige fat biogenesis, stimulates integrin-FAK signaling through αV/β5 and αV/β1 integrins, which are known to associate with CD81 (Chang and Finnemann, 2007; Kim et al., 2018). Accordingly, we hypothesized that CD81 forms a complex with αV/β1 and/or αV/β5 integrins in beige APCs and modulates integrin-FAK signaling in response to irisin. To test this hypothesis, we first examined the protein interactions between CD81 and αV/β1 or αV/β5 integrins by reconstituting these proteins in HEK293T cells. By immunoprecipitating ITGB1 or ITGB5 using a Myc-antibody in these cells, we found that both ITGB1 and ITGB5 interacted with integrin αV and CD81 (Figure 4D).

To test if αV/β1 or αV/β5 integrins in $CD81^+$ APCs are required for FAK signaling in response to irisin, we next isolated $CD81^+$ APCs from Ing WAT of *Itgb1*$^{flox/flox}$ mice in which *Itgb1* was deleted by transducing the cells with a retroviral Cre (Figures 4E and S5B). Subsequently, the *Itgb1* knockout (KO) and control cells (vector) were treated with antagonistic antibodies against ITGB1, ITGB5, or IgG control, prior to irisin treatment. We found that irisin stimulated FAK phosphorylation in control $CD81^+$ APCs, whereas genetic deletion of *Itgb1* or the specific antagonistic antibody against ITGB1 completely blunted the effect of irisin to trigger FAK phosphorylation (Figure 4F). Antibody-based blockade of ITGB5 also potently, though not completely, blunted the irisin-induced FAK phosphorylation in $CD81^+$ APCs. To further probe the genetic requirement of ITGB5 for irisin-induced integrin-FAK signaling, we isolated $CD81^+$ APCs from Ing WAT of *Itgb5* null and wild-type control mice (Figures 4G and S5C). Consistent with the above results, blockade of integrin ITGB1 by its antagonistic antibody completely blocked FAK phosphorylation following irisin treatment. We also found that genetic deletion of *Itgb5* inhibited irisin-induced FAK phosphorylation in $CD81^+$ APCs (Figure 4H). Together, these data indicate that irisin-induced integrin-FAK signaling in $CD81^+$ APCs requires both β1 and β5 integrins.

Next, we examined the extent to which CD81 is required for irisin-induced FAK signaling in the Ing WAT of CRISPRi-*Cd81* mice (Figure S5D). We found that irisin rapidly increased FAK phosphorylation in Lin^- $Sca1^+$ cells isolated from control mice within 5 min after the treatment, but this effect was completely lost in analogous cells from CRISPRi-*Cd81* mice (Figure 4I). Conversely, we found that HEK293T cells ectopically expressing both αV/β5 integrins and CD81 responded to irisin at 1 pM to induce FAK phosphorylation, whereas cells expressing only αV/β5 integrins required irisin at 10 pM or higher, indicating that CD81 sensitized these cells to irisin (Figure S5E). Importantly, irisin at concentrations at or above 1 ng/ml stimulated the proliferation of Lin^- $Sca1^+$ cells from the Ing WAT of control mice but failed to do so in analogous cells from CRISPRi-*Cd81* mice (Figure 4J). These results indicate that CD81 is required for irisin-induced integrin-FAK signaling and APC proliferation.

CD81 Is Required for *De Novo* Beige Fat Biogenesis

Our data highlighting CD81 as a regulator of beige APC proliferation prompted us to ask if CD81 is required for beige fat biogenesis. To this end, CRISPRi-*Cd81* mice and littermate controls were exposed to 8°C temperature for 3 days (Figure 5A). Consistent with the cell proliferation data, the number of proliferative APCs (Lin^-: $Sca1^+$: $Ki67^+$) in the Ing WAT, but not in Epi WAT, of CRISPRi-*Cd81* mice was significantly lower than that of control mice following cold exposure (Figure 5B). These data suggest that CD81 is required for cold-induced APC proliferation in the Ing WAT.

Next, we characterized the formation of cold-induced beige fat in these mice. Cold exposure stimulated the formation of beige adipocytes with multilocular lipid droplets and UCP1 expression in the Ing WAT of control mice. However, cold-induced beige fat biogenesis was strikingly impaired in the Ing WAT of CRISPRi-*Cd81* mice (Figure 5C). Also, CD81 loss significantly reduced the expression of brown/beige fat-selective genes, but not general adipogenic genes and gene encoding β-adrenoceptors, in the Ing WAT following cold exposure (Figure 5D). Of note, we did not observe a notable difference in the expression of thermogenic genes in the iBAT between the genotypes (Figures S6A and S6B). The data are consistent with the results of our *Cd81*-lineage tracing result in which the majority of brown adipocytes in iBAT did not stem from $CD81^+$ APCs. Importantly, OCR in the Ing WAT, but not in the iBAT, of CRISPRi-*Cd81* mice was significantly lower than that of control mice (Figures 5E and S6C). Furthermore, the core body temperatures of CRISPRi-*Cd81* mice were modestly but significantly lower than those of control mice following cold acclimation (Figure 5F), while cold-stimulated muscle shivering was not different between the genotypes (Figures S6D and S6E).

Because CRISPRi-*Cd81* mice lack CD81 in all the cells, we next asked if the reduced beige fat biogenesis in CRISPRi-*Cd81* mice was due to impaired *de novo* beige adipogenesis in $CD81^+$ APCs or reduced reinstallation of the thermogenic program in mature adipocytes. To this end, we generated inducible $CD81^+$ cell-specific *Pparg* KO mice (*Pparg*^{CD81} KO, *Cd81*-Cre^{ERT2}; *Pparg*$^{flox/flox}$), in which peroxisome proliferator-activated receptor-γ (PPARγ) was deleted in $CD81^+$ APCs (Figure 5G). In this mouse model, *de novo* beige adipogenesis in $CD81^+$ APCs would be selectively impaired following tamoxifen treatment, such that we could determine the contribution of

Please cite this article in press as: Oguri et al., CD81 Controls Beige Fat Progenitor Cell Growth and Energy Balance via FAK Signaling, Cell (2020), https://doi.org/10.1016/j.cell.2020.06.021

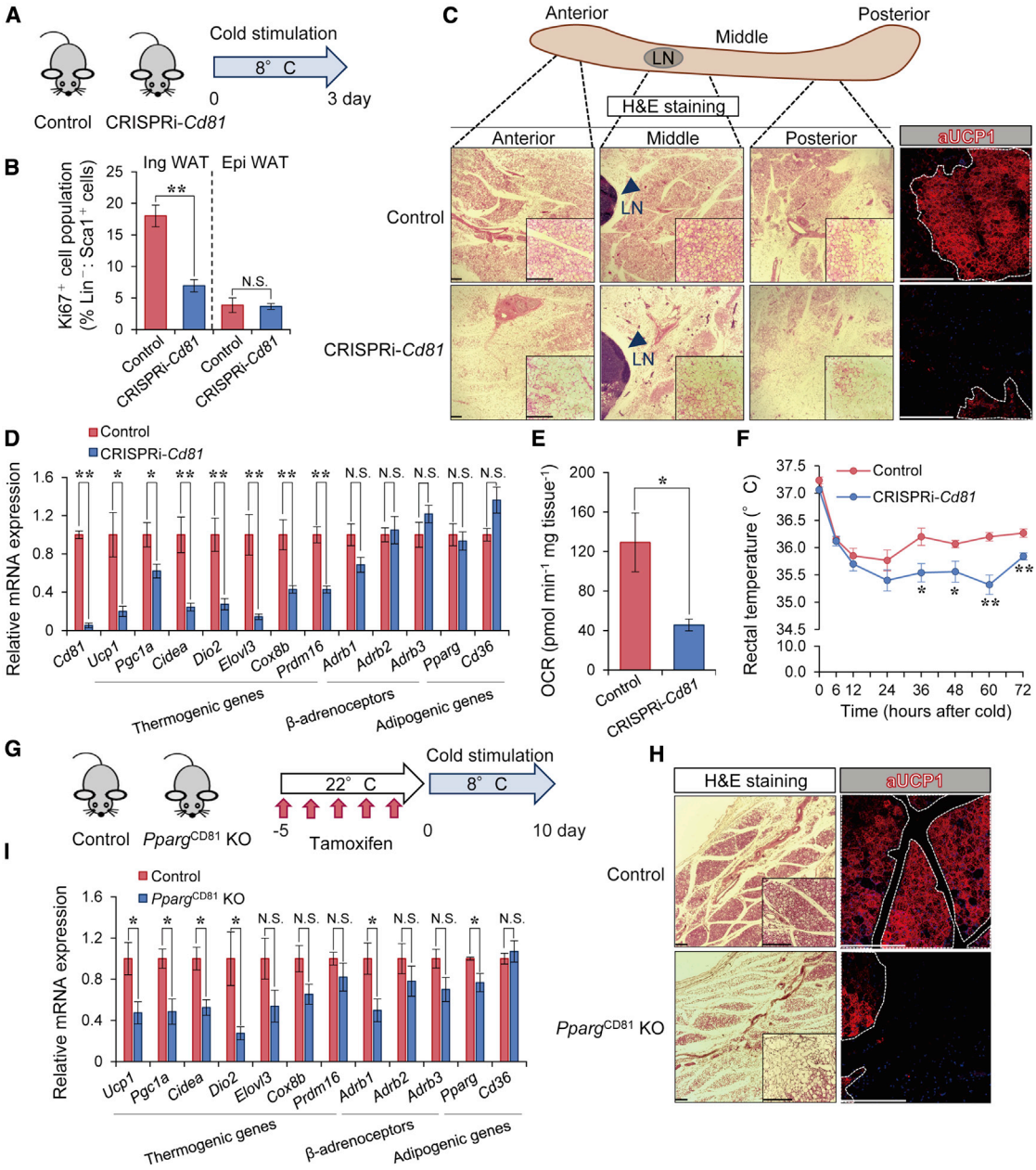

Figure 5. CD81 Is Required for *De Novo* Beige Fat Biogenesis

(A) Illustration of the experiments in (B)–(E).

(B) Ki67$^+$ cells (%) in Lin$^-$: Sca1$^+$ stromal cells from the Ing WAT and Epi WAT in (A). n = 5.

(C) H&E staining and UCP1 immunofluorescent staining in the Ing WAT in (A). Arrowhead indicates lymph node (LN). Scale bar, 200 μm.

(D) mRNA expression of indicated genes in the Ing WAT in (A). n = 5.

(E) OCR in the Ing WAT in (A). Control, n = 3; CRISPRi-*Cd81*, n = 4.

(F) Rectal core body temperature of indicated mice following cold exposure. Control, n = 6; CRISPRi-*Cd81*, n = 5. *p < 0.05, **p < 0.01 by two-way repeated-measures ANOVA with post hoc test by unpaired Student's t test.

(G) Illustration of the experiments in (H) and (I).

(H) H&E staining and UCP1 immunofluorescent staining in the middle region of Ing WAT in (G). Scale bar, 200 μm.

(I) mRNA expression of indicated genes in the Ing WAT in (G). Control, n = 5; *Pparg*^{CD81} KO mice, n = 4. (B, D, E, and I) *p < 0.05, **p < 0.01 by unpaired Student's t test.

Data in (B), (D)–(F), and (I) are represented as mean ± SEM.

Please cite this article in press as: Oguri et al., CD81 Controls Beige Fat Progenitor Cell Growth and Energy Balance via FAK Signaling, Cell (2020), https://doi.org/10.1016/j.cell.2020.06.021

$CD81^+$ APCs to *de novo* beige fat biogenesis. We thus pretreated $Pparg^{CD81}$ KO mice and littermate control mice ($Pparg^{flox/flox}$) with tamoxifen at ambient temperature for 5 consecutive days and subsequently transferred these mice to 8°C for 10 days. Histological analysis of the Ing WAT showed that $Pparg^{CD81}$ KO mice had far fewer beige adipocytes and had lower UCP1 expression than did control mice, although some clusters of multilocular $UCP1^+$ beige adipocytes were observed in $Pparg^{CD81}$ KO mice in the middle region of the Ing WAT (Figures 5H and S6F). Furthermore, mRNA expression of brown/beige fat-selective genes in the Ing WAT of $Pparg^{CD81}$ KO mice was significantly lower than that of control mice (Figure 5I). Together, these results indicate that CD81 is required for cold-stimulated *de novo* beige fat biogenesis and thermogenesis.

CD81 Loss Leads to Diet-Induced Obesity, Glucose Intolerance, and Adipose Tissue Dysfunction

The above data lead us to hypothesize that CD81 would be an important determinant of whole-body energy homeostasis. Of note, several transmembrane tetraspanin proteins, including CD81, are expressed in the exosome membranes, and are often used as exosome markers (Colombo et al., 2014); however, we found that CD81 was dispensable for the formation and release of exosomes (Figure S7A). Thus, the contribution of possible changes in exosome secretion per se to the metabolic phenotype of CRISPRi-*Cd81* mice is most likely negligible. To test how CD81 deficiency affects whole-body energy metabolism, 8-week-old CRISPRi-*Cd81* mice and littermate controls were put on a high-fat diet (HFD, 60% fat) for 8 weeks. We found that CRISPRi-*Cd81* mice gained significantly more body-weight than controls starting at 3 weeks of HFD and thereafter (Figure 6A). The greater body-weight gain in CRISPRi-*Cd81* mice was due to increased lean mass and fat mass (Figure 6B), although neither food intake nor locomotor activity was different between the genotypes (Figure 6C, D). By contrast, CRISPRi-*Cd81* mice had significantly lower whole-body energy expenditure (VO_2) than did control mice: it is important to note that the reduced VO_2 in CRISPRi-*Cd81* mice was detected at 2 weeks of HFD when the differences in body weight had not yet manifest (Figure 6E). Moreover, CRISPRi-*Cd81* mice had a higher respiratory exchange ratio (RER, VCO_2/VO_2) than did control mice, suggesting that CD81 loss causes a fuel switch toward carbohydrate oxidation (Figure 6F). Furthermore, CRISPRi-*Cd81* mice were glucose intolerant relative to control mice after 8 weeks of consuming a HFD (Figure 6G). This phenotype was not due to a metabolic consequence of obesity because glucose intolerance in CRISPRi-*Cd81* mice already emerged within 2 weeks of HFD, a time at which the body weights between the two groups had not yet diverged (Figure S7B). CRISPRi-*Cd81* mice were also insulin-resistant relative to control mice (Figure 6H). In addition, the liver of CRISPRi-*Cd81* mice contained significantly more triglycerides than did those of control mice (Figures 6I and S7C).

We next examined the extent to which CD81 loss alters adipose tissue inflammation. Although macrophages express detectable levels of CD81, the capacity of bone marrow cells to differentiate into macrophages (BMDM) and the ability of these BMDM to express pro-inflammatory markers were not altered by the presence or absence of CD81 (Figures S7D–S7G). The metabolic phenotype of CRISPRi-*Cd81* mice is thus unlikely to be due to an intrinsic hyperactivation of macrophages. However, we found that, in association with their relative obesity, the Ing WAT of CRISPRi-*Cd81* mice expressed significantly higher levels of pro-inflammatory and pro-fibrotic genes than did control mice (Figure 6J). Indeed, analyzing Ing WAT-resident immune cells by FACS showed that obese CRISPRi-*Cd81* mice had significantly more macrophages, neutrophils, monocytes, and eosinophils in the Ing WAT than did control mice fed the same HFD diet, even though the number of total Lin^- $Sca1^+$ cells and other immune cells (B cells, T cells, natural killer [NK] cells) in Ing WAT were similar between the two groups (Figures 6K and S7H). The expression of CD11c, a marker of pro-inflammatory (M1-like) macrophages, was significantly higher in Ing WAT-resident macrophages from CRISPRi-*Cd81* mice than that in control mice, whereas the expression of CD206, an M2-macrophage marker, was not different between the genotypes (Figure 6L). This pro-inflammatory macrophage phenotype was selective to the Ing WAT, as no such differences were seen when examining the Epi WAT (Figures S7I and S7J).

$CD81^+$ APC Enrichment in Human Subcutaneous Fat Correlates Negatively with Metabolic Health

Given the results in mice, we aimed to determine whether the number of $CD81^+$ APCs is associated with any metabolic traits in humans. We first isolated $CD81^+$ APCs from the subcutaneous fat in a cohort of 7 healthy men (age 49 ± 8 years [mean ± SD], BMI 29 ± 6 kg/m^2) with no history of diabetes. For the isolation of $CD81^+$ APCs, we used PDGFRα instead of Sca1 (Lin^-: $PDGFR\alpha^+$: $CD81^+$) because humans lack Sca1, and both PDGFRα and Sca1 mark the same $CD81^+$ APCs in the Ing WAT of mice (Figure 1E). Consistent with our findings in mice, human $CD81^+$ cells (Lin^-: $PDGFR\alpha^+$: $CD81^+$) from the subcutaneous fat of human subjects included a significantly higher number of $Ki67^+$ cells than did corresponding $CD81^-$ cells (Lin^-: $PDGFR\alpha^+$: $CD81^-$), suggesting that human $CD81^+$ APCs in the subcutaneous fat are also a proliferative population (Figure S7K).

Next, we examined human subcutaneous fat from 28 individuals across a wide BMI range that were recruited from a well-described multiethnic cohort of adults assembled in the San Francisco Bay area (Alba et al., 2018). In analyzing the correlation between the number of $CD81^+$ APCs within the subcutaneous fat and metabolic profiles of these individuals (Table S2), we found that the percentage of $CD81^+$APCs significantly correlated inversely with HOMA-IR, fasting blood glucose levels, and diastolic blood pressure (Table 1). Furthermore, we found a significant inverse correlation between the number of subcutaneous fat $CD81^+$ APCs and both absolute visceral fat mass (kg), as measured by dual-energy X-ray absorptiometry (DXA), and visceral adiposity (% VAT /fat mass). There was a trend toward an inverse correlation between $CD81^+$ APC enrichment and both fasting insulin and triglyceride levels, and a trend toward a positive correlation between $CD81^+$ APC enrichment and HDL cholesterol levels, although these did not reach statistical significance. By contrast, there was no correlation with BMI, total fat mass, or total lean mass. It is important to note that no correlations were seen with these metabolic parameters when only

Please cite this article in press as: Oguri et al., CD81 Controls Beige Fat Progenitor Cell Growth and Energy Balance via FAK Signaling, Cell (2020), https://doi.org/10.1016/j.cell.2020.06.021

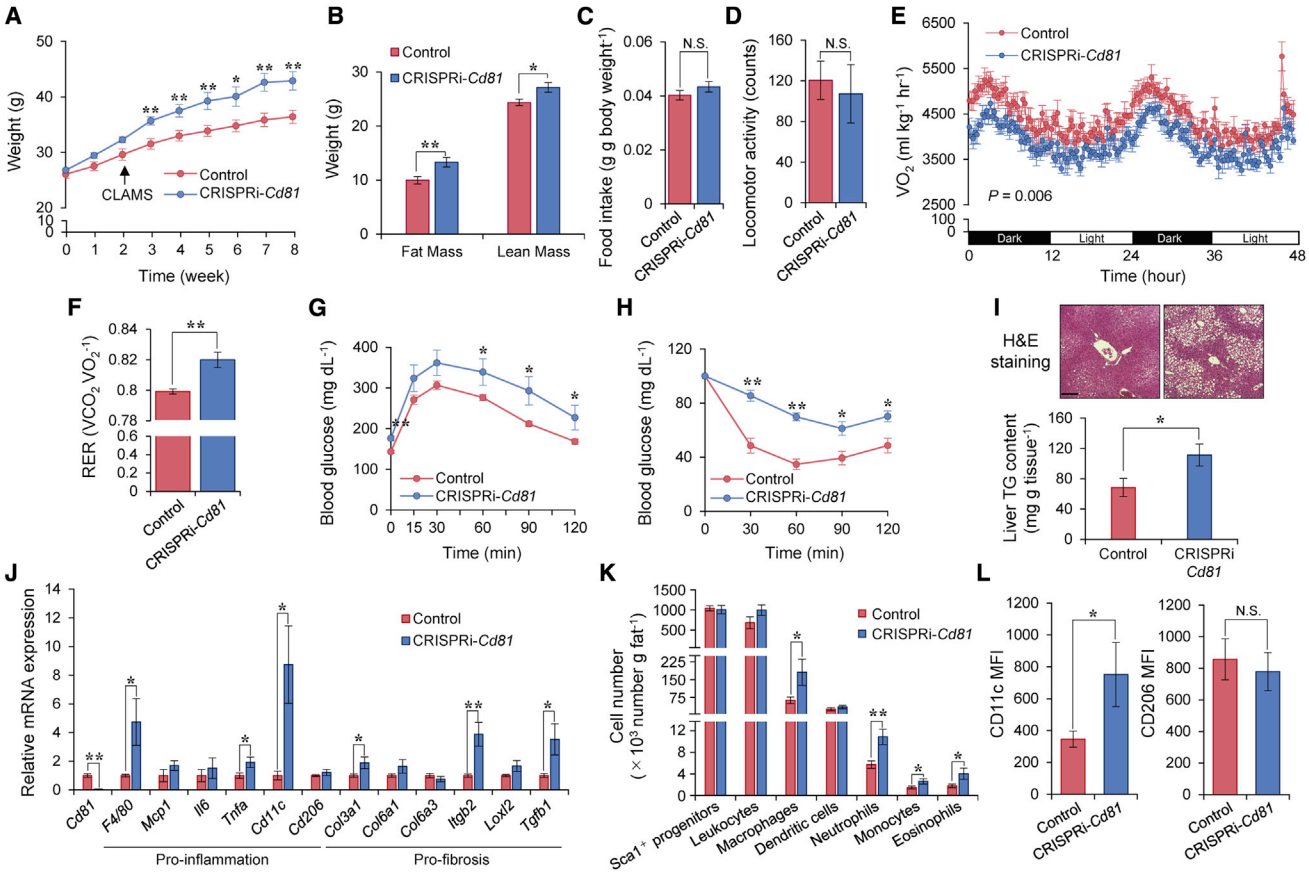

Figure 6. CD81 Loss Causes Obesity, Glucose Intolerance, and Adipose Tissue Inflammation

(A) Body-weight of indicated mice on HFD. Control, n = 9; CRISPRi-*Cd81*, n = 6.

(B) Fat mass and lean mass of mice on 8 weeks of HFD. Control, n = 9; CRISPRi-*Cd81*, n = 6.

(C) Food intake of mice on HFD. Control, n = 8; CRISPRi-*Cd81*, n = 6.

(D) Locomotor activity of mice in (C). (C and D) N.S., not significant by unpaired Student's t test.

(E) Whole-body energy expenditure (VO_2, mL kg^{-1} hr^{-1}) of mice on 2 weeks of HFD. Control, n = 8; CRISPRi-*Cd81*, n = 6. p value by two-way repeated-measures ANOVA.

(F) RER of mice in (E).

(G) GTT in mice on 8 weeks of HFD. Control, n = 9; CRISPRi-*Cd81*, n = 6.

(H) ITT in mice in (G). (A, G, and H) *p < 0.05, **p < 0.01 by two-way repeated-measures ANOVA with post hoc test by unpaired Student's t test.

(I) Top: H&E staining in the liver of mice on 10 weeks of HFD. Sale bar, 200 μm. Bottom: TG contents. Control, n = 9; CRISPRi-*Cd81*, n = 6.

(J) mRNA expression of pro-inflammatory and pro-fibrosis genes in the Ing WAT of mice on 10 weeks of HFD. Control, n = 7; CRISPRi-*Cd81*, n = 6.

(K) The number of total non-leukocyte stromal cells ($CD45^-$: $Sca1^+$), leukocytes ($CD45^+$), macrophages ($CD45^+$: $CD64^+$), dendritic cells ($CD45^+$: $CD64^-$: $CD11c^+$), neutrophils ($CD45^+$: $CD64^-$: $Ly6G^+$), monocytes ($CD45^+$: $CD64^-$: $Ly6C^+$), eosinophils ($CD45^+$: $CD64^-$: $SiglecF^+$) per gram of the Ing WAT of mice on 10 weeks of HFD. Control, n = 8–9; CRISPRi-*Cd81*, n = 5–6.

(L) The expression of M1-like macrophage marker (CD11c) and M2-like macrophage marker (CD206) among total macrophages in the Ing WAT from mice on 10 weeks of HFD. Control, n = 9; CRISPRi-*Cd81*, n = 6. (B, F, I–L) *p < 0.05, **p < 0.01 by unpaired Student's t test.

Data are represented as mean ± SEM.

Lin^- $PDGFR\alpha^+$ cells or Lin^- cells were used in the analyses. Taken together, these data point to reduced numbers of $CD81^+$ APCs within the subcutaneous fat as an indicator of metabolic risk in people, in alignment with the predictions that emanate from our accumulated mouse data.

DISCUSSION

PDGFRα and Sca1 (in mice) are known APC markers, but they are also expressed in many other stromal cells; therefore, what distinguishing beige APCs among other $PDGFR\alpha^+$/$Sca1^+$ stromal cells remained unknown. The present study identified CD81 as a cell surface molecule that marks a unique subset of $PDGFR\alpha^+$/$Sca1^+$ stromal cells that give rise to beige adipocytes *in vivo*. $CD81^+$ APCs in the Ing WAT is highly proliferative and the proliferation is further enhanced by cold exposure. This result is intriguing because previous studies did not detect an increase in EdU incorporation in response to cold exposure or β3-AR agonist treatment when all the $PDGFR\alpha^+$ cells were analyzed in aggregate (Lee et al., 2015; Lee et al., 2012). These results

Please cite this article in press as: Oguri et al., CD81 Controls Beige Fat Progenitor Cell Growth and Energy Balance via FAK Signaling, Cell (2020), https://doi.org/10.1016/j.cell.2020.06.021

Table 1. Correlations between % CD81$^+$ Cells and Clinical Parameters

	% CD81$^+$: PDGFRα$^+$: Lin$^-$ Cells		% PDGFRα$^+$: Lin$^-$ Cells		% Lin$^-$ Cells	
Parameter	Rho	p Value	Rho	p Value	Rho	p Value
BMI (kg/m^2)	−0.132	NS	−0.070	NS	0.014	NS
Fat mass (kg)	0.162	NS	0.043	NS	0.232	NS
Lean mass (kg)	0.010	NS	0.313	NS	0.341	0.076
HOMA-IR[a]	−0.433*	0.024	−0.337	0.086	−0.250	NS
Fasting glucose (mg/dL)[a]	−0.477*	0.012	−0.177	NS	−0.139	NS
Fasting insulin (mIU/L)[a]	−0.376	0.053	−0.375	0.054	−0.230	NS
DBP (mm Hg)	−0.411*	0.030	0.135	NS	−0.223	NS
SBP (mm Hg)	0.238	NS	−0.007	NS	0.179	NS
VAT mass (kg)	−0.393*	0.038	−0.063	NS	−0.140	NS
%VAT/FM	−0.384*	0.044	−0.088	NS	−0.248	NS
Triglycerides (mg/dL)	−0.352	0.066	0.107	NS	−0.175	NS
Total cholesterol (mg/dL)	−0.048	NS	0.092	NS	0.090	NS
LDL cholesterol (mg/dL)	0.002	NS	−0.050	NS	0.073	NS
HDL cholesterol (mg/dL)	0.326	0.090	−0.120	NS	0.139	NS

BMI, body mass index; DBP, diastolic blood pressure; SBP, systolic blood pressure; VAT, visceral adipose tissue; FM, fat mass; NS, not significant. HOMA-IR = fasting insulin (mIU/L) × [fasting blood glucose (mg/dL)/405]. Values are presented as Spearman's coefficients of correlation.
*p values are statistically significant (<0.05). n = 28 subjects included in the analysis.
[a]One subject on insulin was excluded from the analysis.

suggest that a relatively small fraction of PDGFRα$^+$/Sca1$^+$ stromal cells, which are marked by CD81, is proliferative and contributes to *de novo* beige adipogenesis. Our results that selective ablation of PPARγ in CD81$^+$ cells attenuates beige fat biogenesis are aligned with studies that cold-induced beige fat biogenesis occurs through *de novo* differentiation, while some mature adipocytes reinstall the thermogenic program (Shao et al., 2019).

Besides CD81$^+$ APCs, diverse progenitor cells likely contribute to forming beige fat within the Ing WAT. For instance, Lin$^-$ PDGFRα$^+$ MyoD$^+$ myogenic progenitors in the Ing WAT give rise to clusters of beige adipocytes that reside near the lymph nodes and exhibit a unique metabolic profile (a.k.a., g-beige fat) (Chen et al., 2019). These g-beige progenitors are distinct from CD81$^+$ APCs and their differentiation is regulated independently from the β-AR pathway. It is possible that heterogeneous APC populations differentially respond to diverse browning stimuli (e.g., exercise, tissue injury, cachexia, and intermittent fasting), and newly formed beige fat is composed of developmentally and functionally distinct subtypes of beige adipocytes depending on the nature of external cues (e.g., cold versus tissue injury). A better understanding of the mechanisms that define thermogenic fat heterogeneity is a significant area of research in the field.

Importantly, CD81 is more than merely a molecular marker of beige APCs. CD81 is known to form a complex with CD19/CD21-B cell receptors (BCR) and controls BCR signaling (Cherukuri et al., 2004; Mattila et al., 2013). We found that CD81 is required for beige APC proliferation by forming a complex with αV/β1 and αV/β5 integrins and controls integrin-FAK signaling in response to irisin. Furthermore, CD81 loss causes systemic glucose intolerance and insulin resistance. Consistent with these results, fat-selective loss of FAK leads to impaired glucose tolerance and insulin sensitivity (Luk et al., 2017). Because irisin increases upon exercise and acts on adipose tissues, the brain, and bone (Boström et al., 2012; Colaianni et al., 2015; Kim et al., 2018), it will be intriguing to determine the extent to which CD81 mediates exercise-induced metabolic changes in these organs. It is also worth noting that several hormones are known to activate integrin-FAK signaling through an interaction with integrins. For example, angiopoietin-like 4 (ANGPTL4) binds to β1/β5 integrins and modulates FAK signaling (Goh et al., 2010) and increased ANGPTL4 promotes beige fat biogenesis in the inguinal WAT (McQueen et al., 2017). It is thus conceivable that, besides irisin, CD81 mediates the activation of integrin-FAK signaling in response to ANGPTL4 and possibly other hormonal cues.

Selective activation of beige fat biogenesis is accompanied by improved insulin sensitivity, reduced adipose tissue inflammation, and fibrosis (Hasegawa et al., 2018; Ikeda et al., 2017; McDonald et al., 2015; Seale et al., 2011; Shinoda et al., 2015b), implying the possibility that the browning capacity of subcutaneous WAT reflects overall metabolic health. The present study found that the proliferative capacity of CD81$^+$ APCs in the inguinal WAT was higher in 129SVE mice (an obesity/diabetes-resistant strain) relative to that in BL6 mice (an obesity/diabetes-prone strain), while CD81$^+$ APC proliferation declined in aging. Importantly, we found that the number of CD81$^+$ APCs in the subcutaneous fat of human subjects showed an inverse correlation with HOMA-IR, fasting glucose levels, diastolic blood pressure, and visceral adiposity. These results are intriguing given the recent clinical observation that mitochondrial activity in the subcutaneous fat (i.e., mitochondria-enriched adipocytes) correlates inversely with fat inflammation and hyperinsulinemia, and directly with the success of dietary-based weight-loss interventions and fat-specific glucose uptake (Heinonen et al., 2017; Jokinen et al., 2018). Thus, the number of CD81$^+$ APCs in the

subcutaneous fat of people may serve as a useful index to predict the risk of future metabolic disorders or the future success of efforts to control body weight. However, the number of subjects tested in the present study is relatively small, such that the results need to be replicated in larger cohorts under diverse dietary circumstances. Specifically, it will be interesting to explore the potential utility of $CD81^+$ APCs as a biomarker of metabolic responsiveness in the context of weight loss interventions, including bariatric surgery and exercise programs.

STAR★METHODS

Detailed methods are provided in the online version of this paper and include the following:

- KEY RESOURCES TABLE
- RESOURCE AVAILAVILITY
  - Lead Contact
  - Materials Availability
  - Data and Code Availability
- EXPERIMENTAL MODEL AND SUBJECT DETAILS
  - Animals
  - CRISPRi-Cd81 mice
  - Lineage tracing reporter mice
  - Cd81-specific Pparg KO mice
  - Human Subjects
  - Subcutaneous WAT sampling
  - Cells
- METHOD DETAILS
  - scRNA sequencing
  - Transcriptome data analysis
  - Bulk RNA-sequencing and analysis
  - Tissue histology and immunohistochemistry
  - Fluorescence-activated cell sorting (FACS)
  - Human WAT analysis
  - Virus construction
  - Ptk2 KD, Itgb1 KO and Itgb5 KO cells
  - Cell proliferation assay
  - Fat transplantation
  - Metabolic analysis in mice
  - Oxygen consumption assay
  - Protein interaction
  - Irisin-induced FAK signaling in HEK293T cells
  - Immunoblotting
  - Gene expression analysis
- QUANTIFICATION AND STATISTICAL ANALYSIS

SUPPLEMENTAL INFORMATION

Supplemental Information can be found online at https://doi.org/10.1016/j.cell.2020.06.021.

ACKNOWLEDGMENTS

We are grateful to C. Paillart for his support in the CLAMS studies, D. Scheel for histology, and Pollen and Nowakowski for single-cell analysis. This work was supported by the NIH (DK97441 and DK112268 to S.K., DK110098 to K.A., DK110426 and P30DK026687 to K.S., and 5T32HL007374-38 to H.K.) the Edward Mallinckrodt, Jr. Foundation (to S.K.), the National Center for Advancing Translational Sciences, NIH, through UCSF-CTSI (UL1 TR000004 to S.K.K.), the JPB Foundation (to B.M.S.), JSPS Overseas Research Fellowships (to Y.O.), the American Diabetes Association (1-18-PMF-003 to D.L.A.), the Vera M. Long fellowship (to R.N.P.), the Uehara Memorial Foundation (to T.Y.), and a Larry L. Hillblom Foundation fellowship (2019-D-004-FEL to R.D.). Y.O. and K. Tajima were supported by the post-doctoral fellowship from the Manpei Suzuki Diabetes Foundation.

AUTHOR CONTRIBUTIONS

Y.O. and K.S. designed and carried out the overall experiments and analyzed the data. K.S. performed scRNA analyses and bioinformatics. H.K. planned and performed irisin signaling studies with B.M.S. and received technical assistance from C.R.K. D.L.A. performed human adipose tissue experiments and analyzed the data with S.K.K. W.R.B. performed experiments in BMDMs and immune cells with technical assistance from R.T.C. and analyzed data with S.K.K. Q.W. constructed virus experiments and assisted the cellular experiments. Z.B. performed studies in old mice. R.N.P performed bulk RNA analyses and FAK inhibitor studies. K. Tajima, T.Y., K.I., and Y.C. assisted with the animal and cellular experiments. K. Tsujino assisted with studies in *Acta2*-Cre^{ERT2} mice. V.J.G. and M.T.M. developed dCas9-KRAB mice. R.D., C.D.Y., and K.A. assisted with the experiments using *Itgb5* null mice and ITGB antagonistic antibodies. S.K. conceived the project and directed the research. Y.O., K.S., and S.K. wrote the paper with input from all the authors.

DECLARATION OF INTERESTS

The authors declare no competing interests.

Received: December 11, 2019
Revised: March 30, 2020
Accepted: June 9, 2020
Published: July 1, 2020

REFERENCES

Alba, D.L., Farooq, J.A., Lin, M.Y.C., Schafer, A.L., Shepherd, J., and Koliwad, S.K. (2018). Subcutaneous Fat Fibrosis Links Obesity to Insulin Resistance in Chinese Americans. J. Clin. Endocrinol. Metab. *103*, 3194–3204.

Aune, U.L., Ruiz, L., and Kajimura, S. (2013). Isolation and differentiation of stromal vascular cells to beige/brite cells. J. Vis. Exp. (73), 50191.

Berditchevski, F., Zutter, M.M., and Hemler, M.E. (1996). Characterization of novel complexes on the cell surface between integrins and proteins with 4 transmembrane domains (TM4 proteins). Mol. Biol. Cell *7*, 193–207.

Berry, R., and Rodeheffer, M.S. (2013). Characterization of the adipocyte cellular lineage in vivo. Nat. Cell Biol. *15*, 302–308.

Berry, D.C., Jiang, Y., and Graff, J.M. (2016). Mouse strains to study cold-inducible beige progenitors and beige adipocyte formation and function. Nat. Commun. *7*, 10184.

Berry, D.C., Jiang, Y., Arpke, R.W., Close, E.L., Uchida, A., Reading, D., Berglund, E.D., Kyba, M., and Graff, J.M. (2017). Cellular Aging Contributes to Failure of Cold-Induced Beige Adipocyte Formation in Old Mice and Humans. Cell Metab. *25*, 481.

Boström, P., Wu, J., Jedrychowski, M.P., Korde, A., Ye, L., Lo, J.C., Rasbach, K.A., Boström, E.A., Choi, J.H., Long, J.Z., et al. (2012). A PGC1-α-dependent myokine that drives brown-fat-like development of white fat and thermogenesis. Nature *481*, 463–468.

Bredella, M.A., Gill, C.M., Keating, L.K., Torriani, M., Anderson, E.J., Punyanitya, M., Wilson, K.E., Kelly, T.L., and Miller, K.K. (2013). Assessment of abdominal fat compartments using DXA in premenopausal women from anorexia nervosa to morbid obesity. Obesity (Silver Spring) *21*, 2458–2464.

Burl, R.B., Ramseyer, V.D., Rondini, E.A., Pique-Regi, R., Lee, Y.H., and Granneman, J.G. (2018). Deconstructing Adipogenesis Induced by beta3-Adrenergic Receptor Activation with Single-Cell Expression Profiling. Cell Metab. *28*, 300–309.

Please cite this article in press as: Oguri et al., CD81 Controls Beige Fat Progenitor Cell Growth and Energy Balance via FAK Signaling, Cell (2020), https://doi.org/10.1016/j.cell.2020.06.021

Chang, Y., and Finnemann, S.C. (2007). Tetraspanin CD81 is required for the alpha v beta5-integrin-dependent particle-binding step of RPE phagocytosis. J. Cell Sci. *120*, 3053–3063.

Chen, Y., Ikeda, K., Yoneshiro, T., Scaramozza, A., Tajima, K., Wang, Q., Kim, K., Shinoda, K., Sponton, C.H., Brown, Z., et al. (2019). Thermal stress induces glycolytic beige fat formation via a myogenic state. Nature *565*, 180–185.

Cherukuri, A., Shoham, T., Sohn, H.W., Levy, S., Brooks, S., Carter, R., and Pierce, S.K. (2004). The tetraspanin CD81 is necessary for partitioning of coligated CD19/CD21-B cell antigen receptor complexes into signaling-active lipid rafts. J. Immunol. *172*, 370–380.

Chouchani, E.T., and Kajimura, S. (2019). Metabolic adaptation and maladaptation in adipose tissue. Nat. Metab. *1*, 189–200.

Cohen, P., Levy, J.D., Zhang, Y., Frontini, A., Kolodin, D.P., Svensson, K.J., Lo, J.C., Zeng, X., Ye, L., Khandekar, M.J., et al. (2014). Ablation of PRDM16 and beige adipose causes metabolic dysfunction and a subcutaneous to visceral fat switch. Cell *156*, 304–316.

Colaianni, G., Cuscito, C., Mongelli, T., Pignataro, P., Buccoliero, C., Liu, P., Lu, P., Sartini, L., Di Comite, M., Mori, G., et al. (2015). The myokine irisin increases cortical bone mass. Proc. Natl. Acad. Sci. USA *112*, 12157–12162.

Colombo, M., Raposo, G., and Théry, C. (2014). Biogenesis, secretion, and intercellular interactions of exosomes and other extracellular vesicles. Annu. Rev. Cell Dev. Biol. *30*, 255–289.

Fan, J.B., Chen, J., April, C.S., Fisher, J.S., Klotzle, B., Bibikova, M., Kaper, F., Ronaghi, M., Linnarsson, S., Ota, T., et al. (2012). Highly parallel genome-wide expression analysis of single mammalian cells. PLoS ONE *7*, e30794.

Finlin, B.S., Memetimin, H., Confides, A.L., Kasza, I., Zhu, B., Vekaria, H.J., Harfmann, B., Jones, K.A., Johnson, Z.R., Westgate, P.M., et al. (2018). Human adipose beiging in response to cold and mirabegron. JCI Insight *3*, e121510.

Galmozzi, A., Sonne, S.B., Altshuler-Keylin, S., Hasegawa, Y., Shinoda, K., Luijten, I.H.N., Chang, J.W., Sharp, L.Z., Cravatt, B.F., Saez, E., and Kajimura, S. (2014). ThermoMouse: an in vivo model to identify modulators of UCP1 expression in brown adipose tissue. Cell Rep. *9*, 1584–1593.

Goh, Y.Y., Pal, M., Chong, H.C., Zhu, P., Tan, M.J., Punugu, L., Lam, C.R., Yau, Y.H., Tan, C.K., Huang, R.L., et al. (2010). Angiopoietin-like 4 interacts with integrins beta1 and beta5 to modulate keratinocyte migration. Am. J. Pathol. *177*, 2791–2803.

Guerra, C., Koza, R.A., Yamashita, H., Walsh, K., and Kozak, L.P. (1998). Emergence of brown adipocytes in white fat in mice is under genetic control. Effects on body weight and adiposity. J. Clin. Invest. *102*, 412–420.

Hasegawa, Y., Ikeda, K., Chen, Y., Alba, D.L., Stifler, D., Shinoda, K., Hosono, T., Maretich, P., Yang, Y., Ishigaki, Y., et al. (2018). Repression of Adipose Tissue Fibrosis through a PRDM16-GTF2IRD1 Complex Improves Systemic Glucose Homeostasis. Cell Metab. *27*, 180–194.

Heinonen, S., Muniandy, M., Buzkova, J., Mardinoglu, A., Rodríguez, A., Frühbeck, G., Hakkarainen, A., Lundbom, J., Lundbom, N., Kaprio, J., et al. (2017). Mitochondria-related transcriptional signature is downregulated in adipocytes in obesity: a study of young healthy MZ twins. Diabetologia *60*, 169–181.

Hepler, C., Shan, B., Zhang, Q., Henry, G.H., Shao, M., Vishvanath, L., Ghaben, A.L., Mobley, A.B., Strand, D., Hon, G.C., and Gupta, R.K. (2018). Identification of functionally distinct fibro-inflammatory and adipogenic stromal subpopulations in visceral adipose tissue of adult mice. eLife *7*, e39636.

Ikeda, K., Kang, Q., Yoneshiro, T., Camporez, J.P., Maki, H., Homma, M., Shinoda, K., Chen, Y., Lu, X., Maretich, P., et al. (2017). UCP1-independent signaling involving SERCA2b-mediated calcium cycling regulates beige fat thermogenesis and systemic glucose homeostasis. Nat. Med. *23*, 1454–1465.

Jokinen, R., Rinnankoski-Tuikka, R., Kaye, S., Saarinen, L., Heinonen, S., Myohanen, M., Rappou, E., Jukarainen, S., Rissanen, A., Pessia, A., et al. (2018). Adipose tissue mitochondrial capacity associates with long-term weight loss success. Int. J. Obes. (London) *42*, 817–825.

Kajimura, S., Spiegelman, B.M., and Seale, P. (2015). Brown and Beige Fat: Physiological Roles beyond Heat Generation. Cell Metab. *22*, 546–559.

Kim, H., Wrann, C.D., Jedrychowski, M., Vidoni, S., Kitase, Y., Nagano, K., Zhou, C., Chou, J., Parkman, V.A., Novick, S.J., et al. (2018). Irisin Mediates Effects on Bone and Fat via alphaV Integrin Receptors. Cell *175*, 1756–1768.

Koliwad, S.K., Streeper, R.S., Monetti, M., Cornelissen, I., Chan, L., Terayama, K., Naylor, S., Rao, M., Hubbard, B., and Farese, R.V., Jr. (2010). DGAT1-dependent triacylglycerol storage by macrophages protects mice from diet-induced insulin resistance and inflammation. J. Clin. Invest. *120*, 756–767.

Lee, Y.H., Petkova, A.P., Mottillo, E.P., and Granneman, J.G. (2012). In vivo identification of bipotential adipocyte progenitors recruited by β3-adrenoceptor activation and high-fat feeding. Cell Metab. *15*, 480–491.

Lee, Y.H., Petkova, A.P., Konkar, A.A., and Granneman, J.G. (2015). Cellular origins of cold-induced brown adipocytes in adult mice. FASEB J. *29*, 286–299.

Lidell, M.E., Betz, M.J., Dahlqvist Leinhard, O., Heglind, M., Elander, L., Slawik, M., Mussack, T., Nilsson, D., Romu, T., Nuutila, P., et al. (2013). Evidence for two types of brown adipose tissue in humans. Nat. Med. *19*, 631–634.

Lin, J.Z., Rabhi, N., and Farmer, S.R. (2018). Myocardin-Related Transcription Factor A Promotes Recruitment of ITGA5+ Profibrotic Progenitors during Obesity-Induced Adipose Tissue Fibrosis. Cell Rep. *23*, 1977–1987.

Long, J.Z., Svensson, K.J., Tsai, L., Zeng, X., Roh, H.C., Kong, X., Rao, R.R., Lou, J., Lokurkar, I., Baur, W., et al. (2014). A smooth muscle-like origin for beige adipocytes. Cell Metab. *19*, 810–820.

Luk, C.T., Shi, S.Y., Cai, E.P., Sivasubramaniyam, T., Krishnamurthy, M., Brunt, J.J., Schroer, S.A., Winer, D.A., and Woo, M. (2017). FAK signalling controls insulin sensitivity through regulation of adipocyte survival. Nat. Commun. *8*, 14360.

Marcelin, G., Ferreira, A., Liu, Y., Atlan, M., Aron-Wisnewsky, J., Pelloux, V., Botbol, Y., Ambrosini, M., Fradet, M., Rouault, C., et al. (2017). A PDGFRα-Mediated Switch toward $CD9^{high}$ Adipocyte Progenitors Controls Obesity-Induced Adipose Tissue Fibrosis. Cell Metab. *25*, 673–685.

Mather, K.J., Hunt, A.E., Steinberg, H.O., Paradisi, G., Hook, G., Katz, A., Quon, M.J., and Baron, A.D. (2001). Repeatability characteristics of simple indices of insulin resistance: implications for research applications. J. Clin. Endocrinol. Metab. *86*, 5457–5464.

Mattila, P.K., Feest, C., Depoil, D., Treanor, B., Montaner, B., Otipoby, K.L., Carter, R., Justement, L.B., Bruckbauer, A., and Batista, F.D. (2013). The actin and tetraspanin networks organize receptor nanoclusters to regulate B cell receptor-mediated signaling. Immunity *38*, 461–474.

McDonald, M.E., Li, C., Bian, H., Smith, B.D., Layne, M.D., and Farmer, S.R. (2015). Myocardin-related transcription factor A regulates conversion of progenitors to beige adipocytes. Cell *160*, 105–118.

McQueen, A.E., Kanamaluru, D., Yan, K., Gray, N.E., Wu, L., Li, M.L., Chang, A., Hasan, A., Stifler, D., Koliwad, S.K., and Wang, J.C. (2017). The C-terminal fibrinogen-like domain of angiopoietin-like 4 stimulates adipose tissue lipolysis and promotes energy expenditure. J. Biol. Chem. *292*, 16122–16134.

Merrick, D., Sakers, A., Irgebay, Z., Okada, C., Calvert, C., Morley, M.P., Percec, I., and Seale, P. (2019). Identification of a Mesenchymal Progenitor Cell Hierarchy in Adipose Tissue (Science), p. 364.

Muniyappa, R., Lee, S., Chen, H., and Quon, M.J. (2008). Current approaches for assessing insulin sensitivity and resistance in vivo: advantages, limitations, and appropriate usage. Am. J. Physiol. Endocrinol. Metab. *294*, E15–E26.

Ohno, H., Shinoda, K., Spiegelman, B.M., and Kajimura, S. (2012). PPARγ agonists induce a white-to-brown fat conversion through stabilization of PRDM16 protein. Cell Metab. *15*, 395–404.

Oren, R., Takahashi, S., Doss, C., Levy, R., and Levy, S. (1990). TAPA-1, the target of an antiproliferative antibody, defines a new family of transmembrane proteins. Mol. Cell. Biol. *10*, 4007–4015.

Raajendiran, A., Ooi, G., Bayliss, J., O'Brien, P.E., Schittenhelm, R.B., Clark, A.K., Taylor, R.A., Rodeheffer, M.S., Burton, P.R., and Watt, M.J. (2019). Identification of Metabolically Distinct Adipocyte Progenitor Cells in Human Adipose Tissues. Cell Rep. *27*, 1528–1540.

Please cite this article in press as: Oguri et al., CD81 Controls Beige Fat Progenitor Cell Growth and Energy Balance via FAK Signaling, Cell (2020), https://doi.org/10.1016/j.cell.2020.06.021

Sanchez-Gurmaches, J., and Guertin, D.A. (2014). Adipocytes arise from multiple lineages that are heterogeneously and dynamically distributed. Nat. Commun. *5*, 4099.

Schulz, T.J., Huang, T.L., Tran, T.T., Zhang, H., Townsend, K.L., Shadrach, J.L., Cerletti, M., McDougall, L.E., Giorgadze, N., Tchkonia, T., et al. (2011). Identification of inducible brown adipocyte progenitors residing in skeletal muscle and white fat. Proc. Natl. Acad. Sci. USA *108*, 143–148.

Schwalie, P.C., Dong, H., Zachara, M., Russeil, J., Alpern, D., Akchiche, N., Caprara, C., Sun, W., Schlaudraff, K.U., Soldati, G., et al. (2018). A stromal cell population that inhibits adipogenesis in mammalian fat depots. Nature *559*, 103–108.

Seale, P., Conroe, H.M., Estall, J., Kajimura, S., Frontini, A., Ishibashi, J., Cohen, P., Cinti, S., and Spiegelman, B.M. (2011). Prdm16 determines the thermogenic program of subcutaneous white adipose tissue in mice. J. Clin. Invest. *121*, 96–105.

Shao, M., Wang, Q.A., Song, A., Vishvanath, L., Busbuso, N.C., Scherer, P.E., and Gupta, R.K. (2019). Cellular Origins of Beige Fat Cells Revisited. Diabetes *68*, 1874–1885.

Sharp, L.Z., Shinoda, K., Ohno, H., Scheel, D.W., Tomoda, E., Ruiz, L., Hu, H., Wang, L., Pavlova, Z., Gilsanz, V., and Kajimura, S. (2012). Human BAT possesses molecular signatures that resemble beige/brite cells. PLoS ONE *7*, e49452.

Shibue, T., and Weinberg, R.A. (2009). Integrin beta1-focal adhesion kinase signaling directs the proliferation of metastatic cancer cells disseminated in the lungs. Proc. Natl. Acad. Sci. USA *106*, 10290–10295.

Shinoda, K., Luijten, I.H., Hasegawa, Y., Hong, H., Sonne, S.B., Kim, M., Xue, R., Chondronikola, M., Cypess, A.M., Tseng, Y.H., et al. (2015a). Genetic and functional characterization of clonally derived adult human brown adipocytes. Nat. Med. *21*, 389–394.

Shinoda, K., Ohyama, K., Hasegawa, Y., Chang, H.Y., Ogura, M., Sato, A., Hong, H., Hosono, T., Sharp, L.Z., Scheel, D.W., et al. (2015b). Phosphoproteomics Identifies CK2 as a Negative Regulator of Beige Adipocyte Thermogenesis and Energy Expenditure. Cell Metab. *22*, 997–1008.

Su, G., Hodnett, M., Wu, N., Atakilit, A., Kosinski, C., Godzich, M., Huang, X.Z., Kim, J.K., Frank, J.A., Matthay, M.A., et al. (2007). Integrin alphavbeta5 regulates lung vascular permeability and pulmonary endothelial barrier function. Am. J. Respir. Cell Mol. Biol. *36*, 377–386.

Tajima, K., Ikeda, K., Chang, H.Y., Chang, C.H., Yoneshiro, T., Oguri, Y., Jun, H., Wu, J., Ishihama, Y., and Kajimura, S. (2019). Mitochondrial lipoylation integrates age-associated decline in brown fat thermogenesis. Nat. Metab. *1*, 886–898.

Tasic, B., Hippenmeyer, S., Wang, C., Gamboa, M., Zong, H., Chen-Tsai, Y., and Luo, L. (2011). Site-specific integrase-mediated transgenesis in mice via pronuclear injection. Proc. Natl. Acad. Sci. USA *108*, 7902–7907.

Termini, C.M., and Gillette, J.M. (2017). Tetraspanins Function as Regulators of Cellular Signaling. Front. Cell Dev. Biol. *5*, 34.

Tripathi, S., Pohl, M.O., Zhou, Y., Rodriguez-Frandsen, A., Wang, G., Stein, D.A., Moulton, H.M., DeJesus, P., Che, J., Mulder, L.C., et al. (2015). Meta- and Orthogonal Integration of Influenza "OMICs" Data Defines a Role for UBR4 in Virus Budding. Cell Host Microbe *18*, 723–735.

Tsujino, K., Li, J.T., Tsukui, T., Ren, X., Bakiri, L., Wagner, E., and Sheppard, D. (2017). Fra-2 negatively regulates postnatal alveolar septation by modulating myofibroblast function. Am. J. Physiol. Lung Cell. Mol. Physiol. *313*, L878–L888.

van der Lans, A.A., Hoeks, J., Brans, B., Vijgen, G.H., Visser, M.G., Vosselman, M.J., Hansen, J., Jörgensen, J.A., Wu, J., Mottaghy, F.M., et al. (2013). Cold acclimation recruits human brown fat and increases nonshivering thermogenesis. J. Clin. Invest. *123*, 3395–3403.

Vishvanath, L., MacPherson, K.A., Hepler, C., Wang, Q.A., Shao, M., Spurgin, S.B., Wang, M.Y., Kusminski, C.M., Morley, T.S., and Gupta, R.K. (2016). Pdgfrβ+ Mural Preadipocytes Contribute to Adipocyte Hyperplasia Induced by High-Fat-Diet Feeding and Prolonged Cold Exposure in Adult Mice. Cell Metab. *23*, 350–359.

Wang, W., Ishibashi, J., Trefely, S., Shao, M., Cowan, A.J., Sakers, A., Lim, H.W., O'Connor, S., Doan, M.T., Cohen, P., et al. (2019). A PRDM16-Driven Metabolic Signal from Adipocytes Regulates Precursor Cell Fate. Cell Metab. *30*, 174–189.

Wu, J., Boström, P., Sparks, L.M., Ye, L., Choi, J.H., Giang, A.H., Khandekar, M., Virtanen, K.A., Nuutila, P., Schaart, G., et al. (2012). Beige adipocytes are a distinct type of thermogenic fat cell in mouse and human. Cell *150*, 366–376.

Yoneshiro, T., Aita, S., Matsushita, M., Kayahara, T., Kameya, T., Kawai, Y., Iwanaga, T., and Saito, M. (2013). Recruited brown adipose tissue as an antiobesity agent in humans. J. Clin. Invest. *123*, 3404–3408.

Yoneshiro, T., Wang, Q., Tajima, K., Matsushita, M., Maki, H., Igarashi, K., Dai, Z., White, P.J., McGarrah, R.W., Ilkayeva, O.R., et al. (2019). BCAA catabolism in brown fat controls energy homeostasis through SLC25A44. Nature *572*, 614–619.

Young, P., Arch, J.R., and Ashwell, M. (1984). Brown adipose tissue in the parametrial fat pad of the mouse. FEBS Lett. *167*, 10–14.

Please cite this article in press as: Oguri et al., CD81 Controls Beige Fat Progenitor Cell Growth and Energy Balance via FAK Signaling, Cell (2020), https://doi.org/10.1016/j.cell.2020.06.021

STAR★METHODS

KEY RESOURCES TABLE

REAGENT or RESOURCE	SOURCE	IDENTIFIER
Antibodies		
Anti-UCP1 antibody	Abcam	Cat# ab10983; RRID:AB_2241462
Total OXPHOS Rodent WB Antibody Cocktail	Abcam	Cat# ab110413; RRID:AB_2629281
Anti-phospho-FAK (Tyr397) antibody	Cell Signaling Technology	Cat# 3283S; RRID:AB_2173659
Anti-FAK antibody	Cell Signaling Technology	Cat# 3285S; RRID:AB_2269034
Anti-Myc-Tag (9B11) antibody	Cell Signaling Technology	Cat# 2276S; RRID:AB_331783
Anti-HA-tag antibody	Cell Signaling Technology	Cat# 3724; RRID:AB_1549585
Anti-Integrin αV antibody	Cell Signaling Technology	Cat# 60896S; RRID:AB_2753190
Anti-Integrin β1 antibody	Cell Signaling Technology	Cat# 34971S; RRID:AB_2799067
Anti-Integrin β5 antibody	Cell Signaling Technology	Cat# 3629S; RRID:AB_2249358
Anti-β-actin antibody	Sigma-Aldrich	Cat# A3854; RRID:AB_262011
Anti-β-actin antibody [AC-15] (HRP)	Abcam	Cat# ab49900; RRID:AB 867494
Anti-CD81 antibody	Santa Cruz	Cat# sc-166029; RRID:AB_2275892
Anti-CD63 antibody	Santa Cruz	Cat# sc-5275; RRID:AB_627877
Rabbit IgG (H+L) Secondary Antibody	Jackson ImmunoResearch	Cat# 711-035-152; RRID:AB_10015282
Mouse IgG (H+L) Secondary Antibody	Jackson ImmunoResearch	Cat# 715-035-150; RRID:AB_2340770
Anti-PERILIPIN-1 antibody	Abcam	Cat# ab61682; RRID:AB_944751
Anti-GFP antibody	Aves Labs	Cat# GFP-1020; RRID:AB_10000240
Anti-mCherry antibody	Abcam	Cat# ab167453; RRID:AB_ 2571870
APC anti-mouse CD140a Antibody	Biolegend	Cat# 135908; RRID:AB_2043970
Pacific Blue anti-mouse Ly-6A/E (Sca-1) Antibody	Biolegend	Cat# 108120; RRID:AB_493273
APC anti-mouse/rat CD81 Antibody	Biolegend	Cat# 104910; RRID:AB_2562996
PE anti-mouse CD140a Antibody	Biolegend	Cat# 135905; RRID:AB_1953268
PE anti-mouse/human Ki-67 Antibody	Biolegend	Cat# 151209; RRID:AB_2716014
PE Rat Anti-Mouse CD31 Antibody	BD Biosciences	Cat# 553373; RRID:AB_394819
PE CD45 Monoclonal Antibody	eBioscience	Cat# 12-0451-82; RRID:AB_465668
PE anti-mouse TER-119/Erythroid Cells Antibody	Biolegend	Cat# 116207; RRID:AB_313708
PE/Cy7 anti-mouse Ly-6A/E (Sca-1) Antibody	Biolegend	Cat# 122513; RRID:AB_756198
PE/Dazzle 594 anti-mouse CD45 Antibody	Biolegend	Cat# 103145; RRID:AB_2564002
APC anti-mouse F4/80 Antibody	Biolegend	Cat# 123116; RRID:AB_893481
PE anti-mouse CD64 (FcγRI) Antibody	Biolegend	Cat# 139304; RRID:AB_10612740
Brilliant Violet 785 anti-mouse CD11c Antibody	Biolegend	Cat# 117335; RRID:AB_11219204
PerCP/Cy5.5 anti-mouse CD206 (MMR) Antibody	Biolegend	Cat# 141715; RRID:AB_2561991
Brilliant Violet 510 anti-mouse Ly-6C Antibody	Biolegend	Cat# 128033; RRID:AB_2562351
APC/Cy7 anti-mouse Ly-6G Antibody	Biolegend	Cat# 127623; RRID:AB_10645331
APC anti-mouse CD170 (Siglec-F) Antibody	Biolegend	Cat# 155507; RRID:AB_2750236
PE/Cy7 anti-mouse CD3 Antibody	Biolegend	Cat# 100219; RRID:AB_1732068
PerCP anti-mouse CD4 Antibody	Biolegend	Cat# 100537; RRID:AB_893331

(*Continued on next page*)

Please cite this article in press as: Oguri et al., CD81 Controls Beige Fat Progenitor Cell Growth and Energy Balance via FAK Signaling, Cell (2020), https://doi.org/10.1016/j.cell.2020.06.021

Continued

REAGENT or RESOURCE	SOURCE	IDENTIFIER
APC anti-mouse CD8a Antibody	Biolegend	Cat# 100711; RRID:AB_312750
Alexa Fluor® 700 anti-mouse CD19 Antibody	Biolegend	Cat# 115527; RRID:AB_493734
PE anti-mouse IL-23R Antibody	Biolegend	Cat# 150903; RRID:AB_2572188
Brilliant Violet 785 anti-mouse CD335 (NKp46) Antibody	Biolegend	Cat# 137637; RRID:AB_2734201
TruStain FcX PLUS (anti-mouse CD16/32) Antibody	Biolegend	Cat# 156604; RRID:AB_2783138
FITC anti-human CD14 Antibody	Biolegend	Cat# 301803; RRID:AB_314185
FITC anti-human CD31 Antibody	Biolegend	Cat# 303103; RRID:AB_314329
FITC anti-human CD45 Antibody	Biolegend	Cat# 304005; RID:AB_314393
FITC anti-human CD235a (Glycophorin A) Antibody	Biolegend	Cat# 349103; RRID:AB_10612923
PerCP-Cy5.5 Mouse Anti-Human CD140a	BD Biosciences	Cat# 563575; RRID:AB_2738286
APC anti-human CD81 (TAPA-1) Antibody	Biolegend	Cat# 349510; RRID:AB_2564021
PE anti-human Ki-67 Antibody	Biolegend	Cat# 350503; RRID:AB_10660818
Goat anti-Chicken IgY (H+L) Secondary Antibody, Alexa Fluor 488	Thermo Fisher Scientific	Cat# A-11039; RRID:AB_ 2534096
Goat anti-Rabbit IgG (H+L) Highly Cross-Adsorbed Secondary Antibody, Alexa Fluor 488	Thermo Fisher Scientific	Cat# A-11034; RRID:AB_ 2576217
Donkey anti-Rabbit IgG (H+L) Highly Cross-Adsorbed Secondary Antibody, Alexa Fluor 488	Thermo Fisher Scientific	Cat# A-21206; RRID:AB_ 2535792
Goat anti-Rabbit IgG (H+L) Highly Cross-Adsorbed Secondary Antibody, Alexa Fluor 555	Thermo Fisher Scientific	Cat#A-21429; RRID:AB_ 2535850
Goat anti-Rabbit IgG (H+L) Cross-Adsorbed Secondary Antibody, Alexa Fluor 647	Thermo Fisher Scientific	Cat# A-21244 RRID:AB_ 2535812
Donkey anti-Goat IgG (H+L) Cross-Adsorbed Secondary Antibody, Alexa Fluor 647	Thermo Fisher Scientific	Cat# A-21447; RRID:AB_2535864
Anti-Integrin β1 antibody, Clone: HA2/5	BD Biosciences	Cat# 555002; RRID:AB_395636
Anti-Integrin β5 antibody, Clone: ALULA	Su et al., 2007	N/A
Biological Samples		
Human adipose tissues	This paper; Alba et al., 2018	NCT03022682
Chemicals, Peptides, and Recombinant Proteins		
Advanced DMEM/F-12	GIBCO	Cat# 12634-010
autoMACS Rinsing Solution	Miltenyi Biotec	Cat# 130-091-222
CL316,243	Sigma-Aldrich	Cat# C5976
Collagenase D	Roche	Cat# 11088882001
Collagenase from Clostridium histolyticum (Type II)	Sigma-Aldrich	Cat# C6885
Collagenase, Type I, Clostridium histolyticum	Alfa Aesar	Cat# J62406-03
cOmplete, Mini, EDTA-free Protease Inhibitor Cocktail	Roche	Cat# 1836170
Dexamethasone	Sigma-Aldrich	Cat# D4902
Dispase II	Roche	Cat# 04942078001
D-Luciferin, Potassium Salt	Goldbio	Cat# LUCK-100

(*Continued on next page*)

Please cite this article in press as: Oguri et al., CD81 Controls Beige Fat Progenitor Cell Growth and Energy Balance via FAK Signaling, Cell (2020), https://doi.org/10.1016/j.cell.2020.06.021

Continued

REAGENT or RESOURCE	SOURCE	IDENTIFIER
DMEM, high glucose, with L-glutamine	Corning	Cat# 10-017-CV
MesenCult-ACF Plus Medium (Animal component-free medium)	Stem Cell Technologies	Cat# 05449
ERCC ExFold RNA Spike-In Mixes	Thermo Fisher Scientific	Cat# 4456739
Fetal Bovine Serum	Atlanta Biologicals	Cat# S11550
Forskolin	Sigma-Aldrich	Cat# F6886
FreeStyle 293 Expression Medium	GIBCO	Cat# 12338001
Glucose solution	GIBCO	Cat# A2494001
GlutaMAX-I	GIBCO	Cat# 35050-061
HydroMatrix Peptide Cell Culture Scaffold	Sigma-Aldrich	Cat# A6982
Hygromycin B	Thermo Fisher Scientific	Cat# 10687010
Indomethacin	Sigma-Aldrich	Cat# I8280
Insulin	Sigma-Aldrich	Cat# I6634
Isobutylmethylxanthine (IBMX)	Sigma-Aldrich	Cat# I5879
Lipofectamine 2000 Transfection Reagent	Thermo Fisher Scientific	Cat# 11668030
L-(-)-Norepinephrine(+)-bitartrate salt monohydrate	Sigma-Aldrich	Cat# A9512
MACS LS columns	Miltenyi Biotec	Cat# 130-042-401
Non-Adipogenic Progenitor Depletion Cocktail	Miltenyi Biotec	Cat# 130-106-639
Oil Red O	Sigma-Aldrich	Cat# O0625
Oligomycin	Cell Signaling Technology	Cat# 9996
Palmitic acid	Sigma-Aldrich	Cat# P0500
Paraformaldehyde solution 4% in PBS	Santa Cruz Biotechnology	Cat# SC281692
PF-573228	TOCRIS	Cat# 3239
Phosphatase Inhibitor Cocktail 2	Sigma-Aldrich	Cat# P5726
Phosphatase Inhibitor Cocktail 3	Sigma-Aldrich	Cat# P0044
PhosSTOP	Roche	Cat# 04 906 837 001
Anti-c-Myc magnetic beads	Thermo Fisher Scientific	Cat# 88842
Protein A/G magnetic beads	Thermo Fisher Scientific	Cat# 88802
RIPA Lysis and Extraction Buffer	Thermo Fisher Scientific	Cat# 89900
Rosiglitazone	Sigma-Aldrich	Cat# R-2408
RPMI 1640 Medium	GIBCO	Cat# 11875
Sodium Pyruvate	Cell Culture Facility-UCSF	Cat# CCFGE001
SYTOX dead cell stain	Thermo Fisher Scientific	Cat# S34862
Tamoxifen	Sigma-Aldrich	Cat# T5648
Triglycerides Reagent	Thermo Fisher Scientific	Cat# TR22421
TRIzol Reagent	Thermo Fisher Scientific	Cat# 15596026
XF assay medium	Agilent	Cat# 102365-100
0.05% Trypsin 0.53mM EDTA	Corning	Cat# MT25052CI
TrypLE Select	GIBCO	Cat# 12563-029
3,3′,5-Triiodo-L-thyronine	Sigma-Aldrich	Cat# T2877
10 His-tag irisin	Lake Pharma	N/A
Critical Commercial Assays		
Agencourt AMPure XP	Beckman Coulter	Cat# A63880
Agilent High Sensitivity DNA Kit	Agilent	Cat# 5067-4626
C1 Single-Cell Reagent Kit for mRNA Seq	Fluidigm	Cat# 100-6201

(*Continued on next page*)

Please cite this article in press as: Oguri et al., CD81 Controls Beige Fat Progenitor Cell Growth and Energy Balance via FAK Signaling, Cell (2020), https://doi.org/10.1016/j.cell.2020.06.021

Continued

REAGENT or RESOURCE	SOURCE	IDENTIFIER
Click-iT EdU Alexa Fluor 488 Flow Cytometry Assay Kit	Thermo Fisher Scientific	Cat# C10425
exoEasy Maxi Kit	QIAGEN	Cat# 76064
Fixation/Permeabilization Solution Kit	BD Biosciences	Cat# 554714
iscript reverse transcription supermix for rt-qPCR	Bio-Rad	Cat# 1708841
Nextera® XT DNA Sample Preparation Kit	Illumina	Cat# FC-131-1096 and FC-131-1002
Quant-iT PicoGreen® dsDNA Assay Kit	Invitrogen	Cat# P7589
RNeasy Micro Kit	QIAGEN	Cat# 74004
RNeasy Mini Kit	QIAGEN	Cat# 74106
SMARTer Ultra Low RNA Kit for the Fluidigm C1 System, 10 IFCs	Takara Bio, Inc.	Cat# 634833
SMARTer Universal Low Input RNA Kit	Clontech	Cat# 634940
Deposited Data		
Single cell RNA-seq dataset	This paper	ArrayExpress: E-MTAB-8464
Bulk RNA-seq dataset	This paper	ArrayExpress: E-MTAB-8435
Single cell RNA-seq dataset	Hepler et al., 2018	GEO Accession viewer: GSE111588
Experimental Models: Cell lines		
Immortalized inguinal Lin^-: $Sca1^+$: $CD81^+$ cell	This paper	N/A
Experimental Models: Organisms/Strains		
Mouse: C57BL/6J mice	The Jackson Laboratory	000664
Mouse: NU/J mice	The Jackson Laboratory	002019
Mouse: *ThermoMouse;* UCP1-luciferase reporter mice	The Jackson Laboratory	026690
Mouse: *Itgb1*^{loxP} mice	The Jackson Laboratory	004605
Mouse: *Itgb5* null mice	The Jackson Laboratory	004166
Mouse: 129Sv	The Jackson Laboratory	002448
Mouse: 129S6/SvEvTac	Taconic Biosciences	129SVE
Mouse: dCas9-KRAB mice	Tasic et al., 2011	N/A
Mouse: gRNA-*Cd81* transgenic mice	This paper	N/A
Mouse: *Cd81*-Cre^{ERT2} mice	This paper	N/A
Mouse: *Rosa26*-mTmG mice	The Jackson Laboratory	007576
Mouse: *Acta2*-Cre^{ERT2} mice	Tsujino et al., 2017	N/A
Mouse: *Rosa26*-LSL-tdTomato mice	The Jackson Laboratory	007914
Mouse: *Pparg*^{loxP} mice	The Jackson Laboratory	004584
Oligonucleotides		
A full list of qRT-PCR primers, see Table S3	This paper	N/A
Recombinant DNA		
pLKO.1-hygro-*Ptk2*	This paper	N/A
pLKO.1-hygro-shscrambled	This paper	N/A
psPAX2	Addgene	Cat# 12260
pMD2.G	Addgene	Cat# 12259
pMSCV-hygro-Cre	Addgene	Cat# 34565
pEF1-alpha-V	Addgene	Cat# 27290
Human Integrin alpha V/CD51/ITGAV Gene ORF cDNA clone expression plasmid, C-Myc tag	Sino Biological	Cat# HG11269-CM

(*Continued on next page*)

Continued

REAGENT or RESOURCE	SOURCE	IDENTIFIER
Human Integrin beta 1/ITGB1 Gene ORF cDNA clone expression plasmid, C-Myc tag	Sino Biological	Cat# HG10587-CM
Human Integrin beta 5/ITGB5 Gene ORF cDNA clone expression plasmid, C-Myc tag	Sino Biological	Cat# HG10779-CM
Human CD81 cDNA Gene ORF cDNA clone expression plasmid, C-HA tag	Sino Biological	Cat# HG14244-CY
Software and Algorithms		
GENCODE Version M18	The GENCODE Project	https://www.gencodegenes.org/
Kallisto Version 0.46.0	Pachter Lab	https://pachterlab.github.io/kallisto/
R Version 3.5.1	R Development Core Team	https://cran.r-project.org
Tximport Version 1.10.0	Bioconductor	http://bioconductor.org/packages/release/bioc/html/tximport.html
edgeR Version 3.24.0	Bioconductor	https://bioconductor.org/packages/release/bioc/html/edgeR.html
limma Version 3.38.2	Bioconductor	https://bioconductor.org/packages/release/bioc/html/limma.html
Metascape pathway analysis	Tripathi et al., 2015	http://metascape.org
Icy software Version 2.0.0.0	Institut Pasteur and France-BioImaging	http://icy.bioimageanalysis.org/
FlowJo software Version 10.5.3	BD	https://www.flowjo.com/
SPSS Statistics 20.0	IBM	https://www.ibm.com/products/spss-statistics
Other		
High Fat Diet	Research Diets	Cat# D12492

RESOURCE AVAILAVILITY

Lead Contact

Further information and requests for resources and reagents should be directed to and will be fulfilled by the Lead Contact, Shingo Kajimura (skajimur@bidmc.harvard.edu).

Materials Availability

Unique materials and reagents generated in this study are available upon request from the Lead Contact with a completed Materials Transfer Agreement.

Data and Code Availability

The RNA-seq datasets generated during this study are available at ArrayExpress (https://www.ebi.ac.uk) under the accession number E-MTAB-8435 and E-MTAB-8464.

EXPERIMENTAL MODEL AND SUBJECT DETAILS

Animals

All animal experiments were performed according to procedures approved by the Institutional Animal Care and Use Committee for animal care and handling at the University of California, San Francisco (UCSF). C57BL/6J wild-type mice (Stock No. 000664), NU/J mice (Stock No. 002019) and *ThermoMouse* (Stock No. 026690) were obtained from the Jackson Laboratory. *Itgb5* null mice (Stock No. 004166) and *Itgb1*$^{flox/flox}$ mice (Stock No. 004605) available at the Jackson Laboratory were also used for the isolation of CD81^{+} APC. 129SVE mice (129S6/SvEvTac) were obtained from Taconic Biosciences. Male mice were maintained on a standard rodent chow at ambient temperature (22°C) under a 12hour light-dark cycle. Samples were obtained from male mice at 8-16 weeks or 60 weeks of age. For acute cold-exposure study, samples were obtained from male C57BL/6J wild-type mice (8-10 weeks old) at 4°C for 4 days, or male C57BL/6J wild-type mice (8, 24, 40, and 72 weeks old) at 8°C for 5 days using a rodent incubator (Power Scientific, Inc. RIS33SD). For chronic cold exposure, nude mice at 8-10 weeks of age were kept under 12°C for 10 days.

Please cite this article in press as: Oguri et al., CD81 Controls Beige Fat Progenitor Cell Growth and Energy Balance via FAK Signaling, Cell (2020), https://doi.org/10.1016/j.cell.2020.06.021

CRISPRi-Cd81 mice

CRISPRi mice were generated by using a site-specific integrase-mediated approach described previously (Tasic et al., 2011). In brief, CRISPRi mice in the FVB background contain a CAG promoter within the Hipp11 (H11) locus expressing the nuclease-deficient Cas9 fused to the zinc-finger protein 10 (ZNF10) Krüppel-Associated Box (KRAB) repressor domain, together with mCherry and the puromycin resistance. CRISPRi mice were crossed with the FVB mice expressing gRNA-*Cd81* on the H11 locus to generate CRISPRi-*Cd81* mice. Male mice were maintained on a standard rodent chow or a 60% high-fat diet (Research Diets) at ambient temperature (22°C). For cold exposure study, CRISPRi-*Cd81* mice and littermate control mice at 8-10 weeks of age were housed at 8°C for 3 days.

Lineage tracing reporter mice

We inserted Cre^{ERT2} into the *Cd81* gene locus and generated *Cd81*-Cre^{ERT2} mice (Applied StemCell). Subsequently, *Cd81*-Cre^{ERT2} mice were crossed with *Rosa*26-mTmG mice (Jackson Laboratory, Stock No. 007576) to generate *Cd81*-lineage reporter mice (*Cd81*-Cre^{ERT2}; *Rosa26*-mTmG mice). To induce Cre expression in *Cd81*-lineage reporter mice, tamoxifen (Sigma-Aldrich) at 3 mg in 100 μL corn oil per dose were administered intraperitoneally for 5 days. For cold exposure study, male mice (8 weeks old) were kept under 8°C for 14 days. *Rosa26*-mTmG mice without Cre recombinase was used as negative control. *Acta2*-Cre^{ERT2} mice were crossed with *Rosa26*-LSL-tdTomato mice to generate α-SMA^{+} reporter mice (Tsujino et al., 2017). To induce Cre expression in α-SMA^{+} reporter mice, we administered tamoxifen at 2 mg in 100 μL corn oil per dose to male mice at 10 weeks of age for 3 days. At 1 week after tamoxifen treatment, we examined tdTomato expression. *Rosa26*-LSL-tdTomato mice without Cre recombinase was used as negative control.

Cd81-specific Pparg KO mice

To generate CD81^{+} cell-specific *Pparg* knockout mice (*Pparg*^{CD81} KO, *Cd81*-Cre^{ERT2}; *Pparg*$^{flox/flox}$), *Cd81*-Cre^{ERT2} mice were crossed with *Pparg*-floxed mice (Jackson Laboratory, Stock No. 004584). To induce Cre expression, tamoxifen at 3 mg in 100 μL corn oil per dose were administered intraperitoneally for 5 days. For cold exposure study, male *Pparg*^{CD81} KO mice and control mice at 8 weeks of age were housed at 8°C for 10 days.

Human Subjects

All the subjects signed consent forms to participate in the study, which was approved by the University of California, San Francisco (UCSF) Institutional Review Board. Subjects were part of a multiethnic clinical cohort, termed Inflammation, Diabetes, Ethnicity, and Obesity (IDEO), consisting of 25- to 65-year-old healthy men and women living in the San Francisco Bay Area and recruited from medical and surgical clinics at the UCSF and the Zuckerberg San Francisco General Hospital, or through local public advertisements (NCT03022682). The IDEO cohort excludes those taking anti-inflammatory medications, glucocorticoids, or other medications affecting inflammation and those with a history of heart failure, liver failure, renal dysfunction, autoimmune disorders, chronic inflammatory or infectious disease, cancer, or a known history of alcohol or drug abuse. Individuals are also excluded if they have smoked or were not weight stable (> 3% change over 3 months). IDEO collects demographic, medical, medication, dietary, and lifestyle data from subjects using questionnaires. The study involved a random sample of 28 individuals (16 women, 12 men) with BMI > 20 kg/m^2. Eleven subjects had a diagnosis of diabetes (HbA1c > 6.5% or a physician diagnosis plus diabetes medication use). Of these, one individual was taking insulin. Height and weight were measured using a standard stadiometer and scale, with BMI (kg/m^2) calculated from two averaged measurements. Blood pressure was measured with a standard mercury sphygmomanometer on the left arm after at least 10 min of rest. Mean values were determined from two independent measurements.

Blood samples were collected after an overnight fast and analyzed for plasma glucose, insulin, serum total cholesterol, HDL-cholesterol and triglycerides (LDL-cholesterol was estimated according to the Friedwald formula). Insulin resistance was estimated by the homeostatic model assessment of insulin resistance (HOMA-IR) index calculated from fasting glucose and insulin values (Mather et al., 2001; Muniyappa et al., 2008). Subjects taking insulin were excluded from HOMA-IR analyses. Body composition of the subjects was estimated by dual-energy X-ray absorptiometry (DXA) using a Hologic Horizon/A scanner (3-min whole-body scan, < 0.1 G mGy) per manufacturer protocol. A single technologist analyzed all DXA measurements using Hologic Apex software (13.6.0.4:3) following International Society for Clinical Densitometry guidelines. Visceral adipose tissue (VAT) was measured in a 5-cm-wide region across the abdomen just above the iliac crest, coincident with the fourth lumbar vertebrae, to avoid interference from iliac crest bone pixels and matching the region commonly used to analyze VAT mass by CT scan (Bredella et al., 2013).

Subcutaneous WAT sampling

Subcutaneous WAT samples were obtained from the subjects by 2 different methods as described previously (Alba et al., 2018; Hasegawa et al., 2018). In most cases, samples were collected by aspirational needle biopsies using a 14-16 G needle from the peri-umbilical area under local anesthesia. Some of the samples were obtained during elective abdominal or bariatric surgery. WAT samples were freed of visible connective tissue and rinsed to remove blood and clots, after which they were further washed with Krebs-Ringer bicarbonate (KRB) buffer supplemented with 1% BSA. The tissues were rinsed twice in KRB buffer containing 1% BSA and strained using 70 μm nylon filters and immediately placed in KRB buffer containing 1% BSA and 2 mg ml^{-1} Type 1 Collagenase (Alfa Aesar). The tissues were transferred to a 37°C incubator in 50 mL plastic tubes and incubated with agitation for 45-60 min. The digests were washed with KRB buffer containing 1% BSA and strained into fresh 50 mL plastic tubes using 70 μm filters

Please cite this article in press as: Oguri et al., CD81 Controls Beige Fat Progenitor Cell Growth and Energy Balance via FAK Signaling, Cell (2020), https://doi.org/10.1016/j.cell.2020.06.021

to remove any undigested tissue, and the tubes were spun at 450 × g for 10 min at 4°C. The pellets containing the SVF cells were resuspended in RBC lysis buffer for 5-10 min to lyse the RBCs. The resulting SVF cells were further washed with KRB buffer containing 1% BSA at 4°C, and then centrifuged at 450 × g for 10 min at 4°C. The cells were resuspended in freezing medium (90% FBS/10% DMSO) at a concentration of 1.0 × 10^6 cells ml^{-1} cryopreservation medium. The SVF cells were then frozen at −80°C in an ethanol-jacketed closed container overnight, and subsequently stored in liquid nitrogen.

Cells

Mouse stromal vascular fraction (SVF) cells were obtained from male mice by collagenase digestion following the protocol that was published previously (Aune et al., 2013). For the isolation of $CD81^+$ cells for differentiation studies, SVF cells were cultured overnight (~20 hour) before sorting in non-coated plates with DMEM/F12 medium (GIBCO) containing 1% GlutaMAX-I (GIBCO) and 10% FBS (Atlanta Biologicals). Cells were harvested using TrypLE Select (1X) (GIBCO) after washing with PBS. Subsequently, $CD81^-$ (Lin^-: $Sca1^+$: $CD81^-$) and $CD81^+$ APCs (Lin^-: $Sca1^+$: $CD81^+$) were isolated using FACS Aria II and seeded onto collagen-coated plates. Cell plating was scaled according to the surface area. At 95% confluency, cells were induced to differentiate for 2 days with an adipogenic cocktail (0.5 mM IBMX, 2 μg ml^{-1} dexamethasone, 850 nM insulin, 1 nM T3, 125 μM indomethacin with or without 1 μM rosiglitazone) in DMEM/F12 medium containing 1% GlutaMAX-I and 10% FBS (Ohno et al., 2012). Two days after induction, cells were re-fed every 48 hours with adipocyte culture medium containing 1 nM T3, and 850 nM insulin. Cells were fully differentiated by day 6 after induction. Lipid droplets were visualized by Oil-red-O staining. To stimulate thermogenesis, differentiated cells were treated with norepinephrine (NE) at 1 or 10 μM for 4 hours. For protein expression studies, cells were incubated with forskolin at a dose of 10 μM for 6 hours.

For the analysis of integrin-FAK signaling, *Itgb1* KO and *Itgb5* KO $CD81^+$ APCs and Lin^-: $Sca1^+$ cells from CRISPRi-*Cd81* mice were cultured until confluency in non-coated plates in order to reduce basal FAK activity, and induced for 2 days in an adipogenic medium containing 0.5 mM IBMX, 2 μg ml^{-1} dexamethasone, 1 μM rosiglitazone, and 5% FBS. The medium was switched to FreeStyle 293 Expression medium (GIBCO) after washing with warm PBS to starve the cells. After 4 hours of starvation, cells were treated with irisin (Lake Pharma) (Kim et al., 2018) at 100 pM for indicated times. For antagonistic antibody treatment, cells were treated with specific antibodies against integrin β1 (clone: HA2/5, BD Biosciences) or integrin β5 (clone: ALULA) (Su et al., 2007) or mouse IgG as a negative control at 5 μg ml^{-1} for 60 min, followed by irisin treatment for 5 min.

Bone marrow-derived macrophages (BMDMs) were isolated from CRISPRi-*Cd81* and control mice on a high-fat diet for 10 weeks and differentiated as described previously (Koliwad et al., 2010). In brief, male mice were euthanized with Avertin, and their tibias and femurs were flushed of bone marrow. Bone marrow was filtered and cleared of red blood cells with ACK lysis buffer. The bone marrow cells were plated, and the myeloid precursors were differentiated for 6-8 days in RPMI 1640 (GIBCO) containing 10% FBS, 1% penicillin/streptomycin, 1% HEPES, and 10% previously prepared L929-conditioned media to yield BMDMs; media was changed every 2-3 days. To stimulate a pro-inflammatory response, we incubated BMDMs with a metabolic cocktail containing 30 mM glucose, 10 nM insulin, and 0.5 mM palmitic acid for 18 hours. Cells were maintained at 37°C.

METHOD DETAILS

scRNA sequencing

Single-cell RNA extraction and mRNA amplification were performed on the C1 Single-Cell Auto Prep Integrated Fluidic Circuit (IFC) following the methods described in the protocol (PN 100-7168, https://www.fluidigm.com/). For experiments where ERCC ExFold RNA Spike-In were used, the spikes were added to the lysis mix at a 20,000-fold dilution. The PCR thermal protocol was adapted from a publication that optimized template-switching chemistry for single-cell mRNA Seq (Fan et al., 2012) and is outlined in the C1 Single-Cell Auto Prep System protocol. The cDNA reaction products were quantified using the Quant-iT PicoGreen® dsDNA Assay Kit (Invitrogen) and subsequently diluted to a final concentration of 0.15–0.30 ng/μL using C1 Harvest Reagent. The diluted cDNA reaction products were converted into mRNA Seq libraries using the Nextera® XT DNA Sample Preparation Kit (Illumina, FC-131-1096 and FC-131-1002, 1 kit used for 4 C1 IFCs/384 samples) following manufacturer's instructions with minor modifications. Specifically, reactions were run at one-quarter of the recommended volume, the tagmentation step was extended to 10 min, and the extension time during the PCR step was increased from 30 s to 60 s. After the PCR step, samples were pooled, cleaned twice with 0.9X Agencourt AMPure XP SPRI beads (Beckman Coulter), eluted in C1 DNA Dilution Reagent at half of the recommended volume and quantified using a High sensitivity DNA chip (Agilent).

Transcriptome data analysis

Sequenced tags from single-end sequenced libraries for the samples were pseudo-aligned to mouse reference transcriptome built from GENCODE Version M18. Transcript-level abundance estimates were generated using a fast RNA-seq quantification program, Kallisto (Version 0.44.0). All downstream analyses were performed using R (Version 3.5.1). Transcript-level estimates from Kallisto were imported into R and expression levels per gene were estimated using the Bioconductor package tximport (Version 1.10.0). Library size normalization was performed using edgeR (Version 3.24.0). Expression differences between samples were quantified using the limma-voom pipeline (limma Version 3.38.2). In the limma-voom pipeline used for differential gene expression analysis, raw counts were transformed into log2 counts per million, where "per million reads" were defined based on the library normalization

Please cite this article in press as: Oguri et al., CD81 Controls Beige Fat Progenitor Cell Growth and Energy Balance via FAK Signaling, Cell (2020), https://doi.org/10.1016/j.cell.2020.06.021

factors computed by edgeR. A linear model was fitted to the voom normalized data, and comparison between groups, $CD81^+$ and $CD81^-$ was obtained from the linear fitted model. Benjamini-Hochberg procedure was applied in order to control the false discovery rates. Transcriptome data of mouse APCs were analyzed from the recent scRNA sequencing data (GSE111588).

Bulk RNA-sequencing and analysis

Total RNA was isolated from sorted $CD81^+$ and $CD81^-$ cells from wild-type C57BL/6J mice at 10-weeks-old using RNeasy Micro Kit (QIAGEN). For transcriptome data analysis, $CD81^+$ and $CD81^-$ cells were collected without overnight culture. cDNA synthesis and amplification were performed from 50 ng of total RNA using SMARTer® Universal Low Input RNA Kit (Clontech) according to manufacturer's instruction. Sequencing adapters were ligated, and high-throughput sequencing was performed using Illumina HiSeq 3000 instrument at the UCLA Clinical Microarray Core. To compare Fluidigm dataset and sorted bulk $CD81^+$ transcriptome, FASTQ files from the bulk sequencing data were downsampled to 2,700,000 reads, which is the median read depth per cell for the Fluidigm dataset, using Seqtk (https://github.com/lh3/). Both Fluidigm and sorted $CD81^{+/-}$ FASTQ files were pseudoaligned and converted to TPM (Transcripts Per Million) by Kallisto (version 0.46.0) with default parameters. The integrated expression matrix was imported to Seurat and variable genes across the cells were identified by mean.var.plot (y.cutoff = 2,x.low.cutoff = 2). PCA and Hierarchical clustering were performed using the variable genes. The first 20 principal components (PC) were used for clustering. Biological pathway analysis was performed using Metascape (Tripathi et al., 2015).

Tissue histology and immunohistochemistry

For hematoxylin and eosin (H&E) staining, tissues of mice were fixed in 4% paraformaldehyde (PFA) overnight at 4°C, followed by dehydration in 70% ethanol. After the dehydration procedure, tissues were embedded in paraffin, sectioned at a thickness of 5-7 or 15 μm, and stained with H&E following the standard protocol. Images were acquired using a Revolve microscope (ECHO Laboratories). For immunostaining, paraffin-embedded tissues were deparaffinized twice in xylene and subsequently rehydrated. After incubating the slides for 20 min in boiling water, the tissues were blocked in PBS containing 10% goat or donkey serum with 0.1% Tween 20 for 60 min. After washing in PBS, slides were incubated with rabbit anti-UCP-1(1:200, ab10983, Abcam), goat anti-PERILIPIN-1 (1:100, ab61682, Abcam), rabbit anti-mCherry (1:500, ab167453, Abcam), rat anti-PDGFRα (1:100, 135908, Biolegend) and chicken anti-GFP (1:500, GFP-1020, Aves Labs) antibody overnight at 4°C, followed by incubation with fluorescence-conjugated second antibody (1:500, Thermo Fisher) for 60 min at room temperature. Anti-mCherry antibody was used for tdTomato staining. Alexa Fluor 488 antibody was used as a second antibody for GFP, UCP1 in CD81-derived transplant. Alexa Fluor 555 antibody was used as a second antibody for mCherry. Alexa Fluor 647 antibody was used as a second antibody for UCP1 in CRISPRi-*Cd81* mice, *Cd81*-Cre^{ERT2}; *Rosa26*-mTmG mice, $Pparg^{CD81}$ KO mice study and PERILIPIN-1. After washing, the sections were stained with 4',6-diamidino-2-phenylindole (DAPI) and mounted with mounting medium (Cytoseal 60, Thermo Scientific). Images of tissue samples were captured using the Inverted Microscope Leica DMi8 and analyzed using the Icy software (Version 2.0.0.0).

Fluorescence-activated cell sorting (FACS)

For the isolation of $CD81^+$ and $CD81^-$ cells for differentiation studies in culture, adipose tissues from male mice at 8-16 weeks were digested using Collagenase D (1.5 U ml^{-1}) and Dispase II (2.5 U ml^{-1}) to isolate SVF as described previously (Aune et al., 2013), and subsequently cultured overnight (~20 hour) on non-coated plates. The SVF was first gated based on size and granularity. For scRNA sequencing, dead cells were removed based on SYTOX dead cell stain (1:400, Thermo Fisher). A panel of fluorescent antibodies (CD31-PE (1:300, 553373, BD Biosciences), CD45-PE (1:200, 12-0451-82, eBioscience), and TER-119-PE (1:200, 116207, Biolegend)) or MACS® Non-Adipocyte Progenitor Depletion Cocktail for mouse (130-106-639, Miltenyi Biotec) and MACS LS columns (Miltenyi Biotec) were used to deplete $lineage^+$ (Lin^+) cells. The following antibodies were used for the isolation of $CD81^+$ APC (Lin^-: $Sca1^+$: $CD81^+$) in mouse: Sca-1-PB (1:800, 108120, Biolegend) and CD81-APC (1:50, 104910, Biolegend) in autoMACS Rising Solution (Miltenyi Biotec) containing 0.5% BSA in the dark at 4°C for 15 min. This sorting strategy was used to isolate $CD81^+$ APC from C57BL/6J wild-type, 129SVE mice, *ThermoMouse*, *Itgb5* null mice, 129 Sv mice and $Itgb1^{flox/flox}$ mice, and Lin^-: $Sca1^+$ stromal cells from CRISPRi-*Cd81* mice and control mice. CD140a-PE (1:200, 135905, Biolegend) was used to co-stain $PDGFR\alpha^+$ with $Sca1^+$.

To evaluate $CD81^+$ APC number in young versus aged mice, stromal cells were isolated from the SVFs of Ing WAT of young mice (8-10 weeks old) and old mice (60 weeks old) without overnight culture. For intracellular staining, stromal cells were isolated from the SVFs of Ing WAT or Epi WAT without overnight culture. Cells were stained with above antibodies and fixed in 4% PFA for 15 min. Subsequently, cells were incubated in autoMACS Rising Solution containing 0.5% BSA and 0.1% saponin for 15 min and stained with Ki67-PE antibody for 30 min (1:300, 151209, Biolegend). Cell population (%) was calculated as frequency of parent. All the cells were isolated and analyzed using FACS Aria II equipped with 100 μm nozzle diameter. FlowJo software (version 10.5.3) was used for data analysis.

To identify immune cell, Ing WAT and Epi WAT were digested with Type II Collagenase (Sigma-Aldrich) at 2 mg ml^{-1} for 40 min at 37°C while shaking at 200 rpm. The SVF, containing immune cells and progenitors, was pelleted and separated from floating adipocytes by centrifugation at 800 × g for 8 min at 4°C. Red blood cells were lysed with ACK buffer for 3 min on ice. Cells were then filtered and blocked in TruStain FcX PLUS (1:200, 156604, Biolegend) before proceeding to staining for specific markers to be assessed by FACS. The following antibodies were used to identify immune cell in mouse: Sca-1-PECy7 (1:400, 122513, Biolegend), CD45-PE-Dazzle594 (1:4,000, 103145, Biolegend), F4/80-APC (1:400, 123116, Biolegend), CD64-PE (1:400, 139304, Biolegend),

Please cite this article in press as: Oguri et al., CD81 Controls Beige Fat Progenitor Cell Growth and Energy Balance via FAK Signaling, Cell (2020), https://doi.org/10.1016/j.cell.2020.06.021

CD11c-BV785 (1:400, 117335, Biolegend), CD206-PerCP-Cy5.5 (1:400, 141715, Biolegend), Ly6C-BV510 (1:400, 128033, Biolegend), Ly6G-APC-Cy7 (1:400, 127623, Biolegend), SiglecF-APC (1:400, 155507, Biolegend), CD3-PE-Cy7 (1:400, 100219, Biolegend), CD4-PerCP (1:400, 100537, Biolegend), CD8a-APC (1:400, 100711, Biolegend), CD19-A700 (1:400, 115527, Biolegend), IL-23R-PE (1:400, 150903, Biolegend), NKp46-BV785 (1:400, 137637, Biolegend) in PBS containing 1% FBS and 2 mM EDTA in the dark at 4°C for 30 min. DAPI was added immediately prior to analysis to remove dead cells. The SVF was first gated based on size and granularity. This sorting strategy was used to identify immune cells from CRISPRi-*Cd81* mice and control mice on a high-fat diet.

Human WAT analysis

Prior to FACS analysis, individual cryovials of cells were rapidly thawed in a 37°C water bath (1–2 min agitation), resuspended in pre-warmed animal component-free medium (Stem Cell Technologies) and seeded into separate wells of a six-well plate for 72 hours of incubation at 37°C. Cells were pooled, harvested by trypsinization with TrypLE Select, washed with culture medium and resuspended in autoMACS Rising Solution containing 0.5% BSA. The following antibodies were used for the isolation of CD81$^+$ APC (Lin$^-$: PDGFRα^+: CD81$^+$) from subcutaneous WAT in human: CD14-FITC (1:400, 301803, Biolegend), CD31-FITC (1:200, 303103, Biolegend), CD45-FITC (1:200, 304005, Biolegend), CD235a-FITC (1:500, 349103, Biolegend), PDGFRα (CD140a)-PerCP-Cy5.5 (1:200, 563575, BD Biosciences) and CD81-APC (1:500, 349510, Biolegend) in autoMACS Rising Solution containing 0.5% BSA in the dark at 4°C for 15 min. This sorting strategy was used to evaluate the correlations between CD81$^+$ APC and clinical parameters. For intracellular staining, isolated SVF cells were stained with above antibodies without overnight culture, and immediately fixed by using Fixation/Permeabilization Solution Kit (BD Biosciences) as described protocol and stained with Ki67-PE antibody for 30 min (1:500, 350503, Biolegend). Cell population (%) was calculated as frequency of parent.

Virus construction

We generated lentiviral shRNA constructs in pLKO.1-hygromycin (#24150, Addgene) that expressed shRNA targeting mouse *Ptk2* (CCTGGCATCTTTGATATTATA) or scrambled control (CAACAAGATGAAGAGCACCAA) based on the previous study (Shibue and Weinberg, 2009). For virus production, HEK293T packaging cells were transfected with 10 μg of lentiviral plasmids and 10 μg the packaging constructs (psPAX2 and pMD2.G) using a calcium phosphate method. After 48 hours of incubation, the viral supernatant was collected and filtered.

Ptk2 KD, Itgb1 KO and Itgb5 KO cells

For the generation of *Ptk2* knockdown (KD) cells, immortalized Lin$^-$: Sca1$^+$: CD81$^+$cells from Ing WAT by using the SV40 Large T antigen as described previously (Shinoda et al., 2015a) were infected with pLKO.1-shRNA targeting *Ptk2* or scrambled control, followed by hygromycin selection (150 μg ml^{-1}). The knockdown efficiency was confirmed by immunoblotting for FAK. For the generation of *Itgb1* KO cells, CD81$^+$ APCs were isolated from the Ing WAT of *Itgb1*$^{flox/flox}$ mice after overnight culture and subsequently infected with retrovirus constructs expressing Cre (#34565, Addgene) or an empty vector control, followed by hygromycin selection. For the generation of *Itgb5* KO cells, CD81$^+$ cells were isolated from Ing WAT of *Itgb5* null mice and wild-type mice (129 Sv) as control after overnight culture. By immunoblotting, we confirmed that both *Itgb1* KO and *Itgb5* KO cells did not express ITGB1 and ITGB5, respectively.

Cell proliferation assay

To examine changes in APC proliferation *in vivo*, we administered EdU (25mg kg^{-1} body weight, I.P.) to C57BL/6J mice that were acclimated at 22°C or 4°C for 4 days. Two hours after EdU administration, mice were sacrificed and CD81$^+$ APCs from the Ing WAT were isolated for analysis. EdU positive cells were detected by using Click-iT EdU Alexa Fluor 488 Flow Cytometry Assay Kit (Thermo Fisher) and FACS Aria II. For cell proliferation assay in CD81$^-$ cells and CD81$^+$ cells, cells were isolated from Ing WAT or Epi WAT without overnight culture at the sorting day by FACS and seeded directly onto 24-well non-coated plates. Isolated cells were cultured for 5 days in DMEM/F12 medium containing 1% GlutaMAX-I and 10% FBS and re-fed every 48 hours with culture medium. Cell proliferation rate (% growth day^{-1}) were calculated as relative values to the growth rate of CD81$^-$ cells from C57BL/6J mice at 8-10 weeks or 12 weeks of age. For cultured cell proliferation assays, Lin$^-$: Sca1$^+$ cells were isolated from the SVFs of Ing WAT of CRISPRi-*Cd81* mice and littermate control mice at 10-12 weeks of age after overnight culture. To verify cell culture conditions, isolated Lin$^-$: Sca1$^+$ cells were cultured in non-coated plates or collagen-coated plates with cell culture medium. Cell proliferation rate (% growth day^{-1}) were calculated as relative values to the growth rate of control cell on non-coated culture plates. To test the involvement of FBS concentration, isolated Lin$^-$: Sca1$^+$ cells were cultured in non-coated plates with cell culture medium containing FBS at indicated concentrations (0%–20%) for 5 days. Cell proliferation rate (% growth day^{-1}) were calculated as relative values to the growth rate of control cell under the condition of 10% FBS. For irisin experiments, isolated Lin$^-$: Sca1$^+$ cells were treated with irisin at indicated doses (1-10 ng ml^{-1}) for 5 days in DMEM/F12 medium containing 1% GlutaMAX-I and 10% FBS. The culture medium was replaced every 48 hours. Cell proliferation rate (% growth day^{-1}) were calculated as relative values to the growth rate of control cells without irisin treatment. For FAK inhibitor experiments in control and *Ptk2* KD cell, CD81$^+$ APCs were treated with FAK inhibitor (PF-573228, TOCRIS) ranging from 5 nM to 100 nM or vehicle (DMSO) for 4 days in DMEM (Corning) containing 5% FBS. For the FAK inhibitor experiments in CD81$^+$ cell and Lin$^-$: Sca1$^+$ cells, cells were treated with FAK inhibitor at 1 μM or vehicle (DMSO) for

Please cite this article in press as: Oguri et al., CD81 Controls Beige Fat Progenitor Cell Growth and Energy Balance via FAK Signaling, Cell (2020), https://doi.org/10.1016/j.cell.2020.06.021

4 days in DMEM/F12 medium containing 1% GlutaMAX-I and 10% FBS. Culture media containing FAK inhibitor or vehicle were replaced every 24 hours. Cell proliferation rate (% growth day^{-1}) were calculated as relative values to the growth rate of vehicle control cells. To harvest cells, cells were incubated with 0.05% trypsin-EDTA (Corning) at 37°C after washing with PBS. After neutralization with cell culture medium, cells were collected in 1.7 mL tubes. The wells were washed with cell culture medium one more time and then collected in same tube. After centrifugation at 300 × g for 5 min, cell pellets were resuspended in 100 μL of cell culture medium. Cell number was counted using a cell counter.

Fat transplantation

CD81$^-$ and CD81$^+$ APCs were isolated from the Ing WAT of *ThermoMouse* (Galmozzi et al., 2014) following overnight culture. Cells were cultured for 2 days under an adipogenic condition that contains 1 μM rosiglitazone. Subsequently, cells were gently collected using cell scraper and resuspended in a cell culture medium. Cells were implanted with 0.25% HydroMatrix Peptide Cell Culture Scaffold (Sigma-Aldrich). Cells (2 × 10^6 cells) mixed in HydroMatrix (200 μl) were injected subcutaneously into nude mice. Three days after transplantation, mice were kept under 12°C for 10 days. Mice were injected with rosiglitazone (10 mg kg^{-1} body weight) twice daily for 3 days from day 10 to 12. Luciferase activity was monitored at 3, 6, and 13 days after transplantation using an IVIS Spectrum Instrument (Caliper Life Sciences), as described previously (Galmozzi et al., 2014). Images were collected starting 15 min after injection of luciferin (150 mg kg^{-1} body weight, Goldbio). For acute stimulation, β3 adrenergic receptor agonist (CL-316, 243, Sigma-Aldrich) at 1 mg kg^{-1} body weight was injected intraperitoneally 5 hours before harvesting the transplanted fat pads. To examine the transcriptional profile of CD81-derived fat transplants, CD81$^+$ APCs were isolated from the Ing WAT of C57BL/6J mice following overnight culture. Three days after transplantation, mice were kept under 12°C for 10 days. Mice were injected with rosiglitazone (10 mg kg^{-1} body weight) twice daily for 10 days from day 4 to 13. Transplanted fats were isolated for RNA extraction and transcriptional analyses by qRT-PCR. As comparisons, we included Ing WAT samples from wild-type mice under a thermoneutral condition (30°C) for 14 days and cold-acclimated mice at 8°C for 3 days.

Metabolic analysis in mice

CRISPRi-*Cd81* mice and littermate control mice were fed a 60% high-fat diet (HFD, Research Diets) under the ambient temperature condition. HFD feeding was started when mice were 8 weeks old. Whole-body energy expenditure, respiratory exchange ratio (RER), food intake, and locomotor activity (beam break counts) were monitored by a comprehensive lab animal monitoring system (CLAMS) (Columbus Instruments). Metabolic data were collected in mice on a HFD for 2 weeks at 22°C. Body-weight was monitored once a week. Fat mass and lean mass were measured by Body Composition Analyzer EchoMRI (Echo Medical Systems) at 8 weeks of HFD. The rectal temperature was monitored using a TH-5 thermometer (Physitemp). Electromyography (EMG) was recorded for 15 min at 30°C before cold stimulation, and for another 15 min at 8°C after the 3 days cold exposure, following our protocol (Chen et al., 2019; Yoneshiro et al., 2019). For glucose tolerance tests, mice on HFD for 2 or 8 weeks received an intraperitoneal injection of glucose (1.5 g kg^{-1} body weight) after 6 hours of fasting. For insulin tolerance tests, mice on HFD for 8 weeks received an intraperitoneal injection of insulin (1.0 U kg^{-1} body weight) after 3 hours of fasting. Blood samples were collected at several time points after injection, and glucose levels were measured using blood glucose test strips (Abbott). To measure liver triglyceride contents, liver tissues were homogenized in 350 μL ethanolic KOH (100% EtOH: 30% KOH = 2:1) and incubated at 55°C overnight. Subsequently, tissue lysates were brought volume to 1 mL with 50% EtOH. After centrifugation, the supernatant was incubated with 1 M $MgCl_2$ on ice for 10 min. Amounts of triglycerides were determined by an Infinity Triglycerides kit (Thermo Fisher). Exosome were isolated from serum at 8 weeks of HFD using exoEasy Maxi Kit (QIAGEN).

Oxygen consumption assay

OCR in cultured adipocytes and isolated adipose tissue were measured using the Seahorse XFe Extracellular Flux Analyzer (Agilent) in a 24-well plate. CD81$^-$ and CD81$^+$ cells were isolated from the SVFs of Ing WAT after overnight culture. Cells were differentiated as described above and maintained in XF assay medium supplemented with 1 mM sodium pyruvate, 2 mM GlutaMAX-I, and 25 mM glucose. For measurement of NE-induced respiration in cultured adipocytes, cells were treated with 10 μM NE during OCR measurement. For the measurement of uncoupled respiration in differentiated adipocytes, cells were stimulated with NE treatment and subsequently treated with 10 μM oligomycin. For tissue respiration analyses, punch-biopsy tissues of Ing WAT (1.5 mg) or iBAT (1.0 mg) were placed into XFe24 Islet Capture Microplates. OCR in Ing WAT and iBAT were measured 1 hour after incubation with assay medium supplemented with 1 mM sodium pyruvate, 2 mM GlutaMAX-I, and 25 mM glucose.

Protein interaction

HEK293T cells were transfected with the plasmids containing gene of CD81 (#HG14244-CY, Sino Biological), Integrin αV (#27290, Addgene), Integrin β1 (#HG10587-CM, Sino Biological) or Integrin β5 (#HG10779-CM, Sino Biological) using Lipofectamine 2000 according to the manufacture's manual. Twenty-four hours after transfection, medium was switched to FreeStyle 293 Expression medium and cells were incubated for 4 hours. Subsequently, cells were harvested in cold PBS and resuspended in cell lysis buffer (50 mM Tris-HCl pH7.5, 150 mM NaCl, 1 mM $MgCl_2$, 0.1 mM $CaCl_2$, 0.5% Brij98) containing phosphatase inhibitors (Roche) and protease inhibitors (Roche). Cell lysates were rotated for 1 hour at 4°C and then supernatants were collected after centrifugation at 17,000 × g for 10 min. The obtained lysates were rotated with protein A/G magnetic beads (Thermo Fisher) for 20 min at 4°C. After

centrifugation at 1,000 × g for 2 min, the supernatants were subjected to anti-c-Myc magnetic beads (Thermo Fisher) and rotated overnight at 4°C. After washing in the buffer (50 mM Tris-HCl pH7.5, 150 mM NaCl, 1 mM $MgCl_2$, 0.1 mM $CaCl_2$, 0.5% Brij98) three times, precipitated proteins were eluted by boiling with 1 × Laemmli buffer. Each protein was detected by immunoblotting.

Irisin-induced FAK signaling in HEK293T cells

Cells were treated and homogenized as reported (Chang and Finnemann, 2007; Kim et al., 2018). Briefly, HEK293T cells were transfected with the plasmids containing gene of CD81, Integrin αV (#HG11269-CM, Sino Biological) or Integrin β5 using Lipofectamine 2000 according to the manufacture's protocol. Twenty-four hours after transfection, medium was switched to FreeStyle 293 Expression medium and cells were incubated for 4 hours. Subsequently, cells were treated with irisin protein for 5 min and harvested in RIPA buffer. Protein levels of phospho-FAK (Tyr397), FAK, CD81, integrin αV, integrin β5 and β-actin were visualized by immunoblot analysis.

Immunoblotting

Cells and tissues were lysed in RIPA lysis and extraction buffer (Thermo Fisher), phosphatase inhibitors (Sigma-Aldrich) and protease inhibitors (Roche). Total protein lysates were boiled with Laemmli sample buffer containing 355 mM β-mercaptoethanol, loaded on a 4%–12%, 4%–15% or 8% SDS-PAGE. Subsequently, separated proteins were transferred onto PVDF membranes. PVDF membrane blots were blocked in 5% milk or 3%–5% BSA in Tris-buffered saline with Tween 20 (TBS-T) for 1 hour at room temperature and incubated overnight at 4°C with rabbit anti-UCP-1 (1:1,000, ab10983, Abcam), anti-phospho-FAK (Tyr397) (1:1,000, 3283S, Cell Signaling), anti-FAK (1:1,000, 3285S, Cell Signaling), anti-Integrin αV (1:1,000, 60896S, Cell Signaling), anti-Integrin β1 (1:1,000, 34971S, Cell Signaling), anti-Integrin β5 (1:1,000, 3629S, Cell Signaling), anti-HA-tag (1:1,000, 3724, Cell Signaling), mouse anti-Myc-tag (9B11) (1:1,000, 2276S, Cell Signaling), anti-CD81 (1:100, sc-166029, Santa Cruz), anti-CD63 (1:200, sc-5275, Santa Cruz), or anti-β-actin (1:10,000, A3854, Sigma-Aldrich or ab49900, Abcam). Mitochondrial proteins were detected using MitoProfile Total OXPHOS Rodent Antibody Cocktail (1:1,000, ab110413, Abcam). Anti-rabbit IgG (711-035-152, Jackson ImmunoResearch) was used to a second antibody for UCP1, phospho-FAK (Tyr397), FAK, integrin αV, integrin β1, integrin β5, and HA-tag. Anti-mouse IgG (715-035-150, Jackson ImmunoResearch) was used as a secondary for Myc-tag, CD81, CD63, and Total OXPHOS Rodent Antibody Cocktail.

Gene expression analysis

Total RNA was extracted from tissue or cells using TRIzol reagents (Thermo Fisher) followed by the RNeasy Mini Kit (QIAGEN) protocol. Complementary DNA was synthesized using the iScript cDNA Synthesis Kit (Bio-Rad Laboratories) according to the provided protocol. Quantitative RT-PCR was performed using an ABI ViiA 7 PCR cycler (Applied Biosystems). Quantity of a particular gene in each sample was normalized to the TATA-binding protein, *36B4* or *Hprt*. Relative mRNA levels were determined by the ΔΔ Ct method and normalized to an internal calibrator specific to each gene using the formula $2^{-\Delta\Delta CT}$. Primer sequences are provided in Table S3.

QUANTIFICATION AND STATISTICAL ANALYSIS

Statistical analyses were performed using statistical software (SPSS 20.0, IBM). All data were represented as mean ± SEM, except where noted. Unpaired Student's t test was used for two-group comparisons. One-way ANOVA followed by Bonferroni's-test was used for multiple group comparisons. One-way ANOVA followed by Dunnett's-test was used for cell proliferation studies. Unpaired Student's t test with Bonferroni's correction was used for cell proliferation studies and transplantation results. Two-way repeated-measures ANOVA was used for cell proliferation assay results, cold tolerance test results, body weight results, whole-body energy expenditure results, GTT results, and ITT results. Correlations were examined with non-parametric Spearman correlation test. $p < 0.05$ was considered significant in all the experiments. The statistical parameters and the number of mice used per experiment are found in the figure legends.

Supplemental Figures

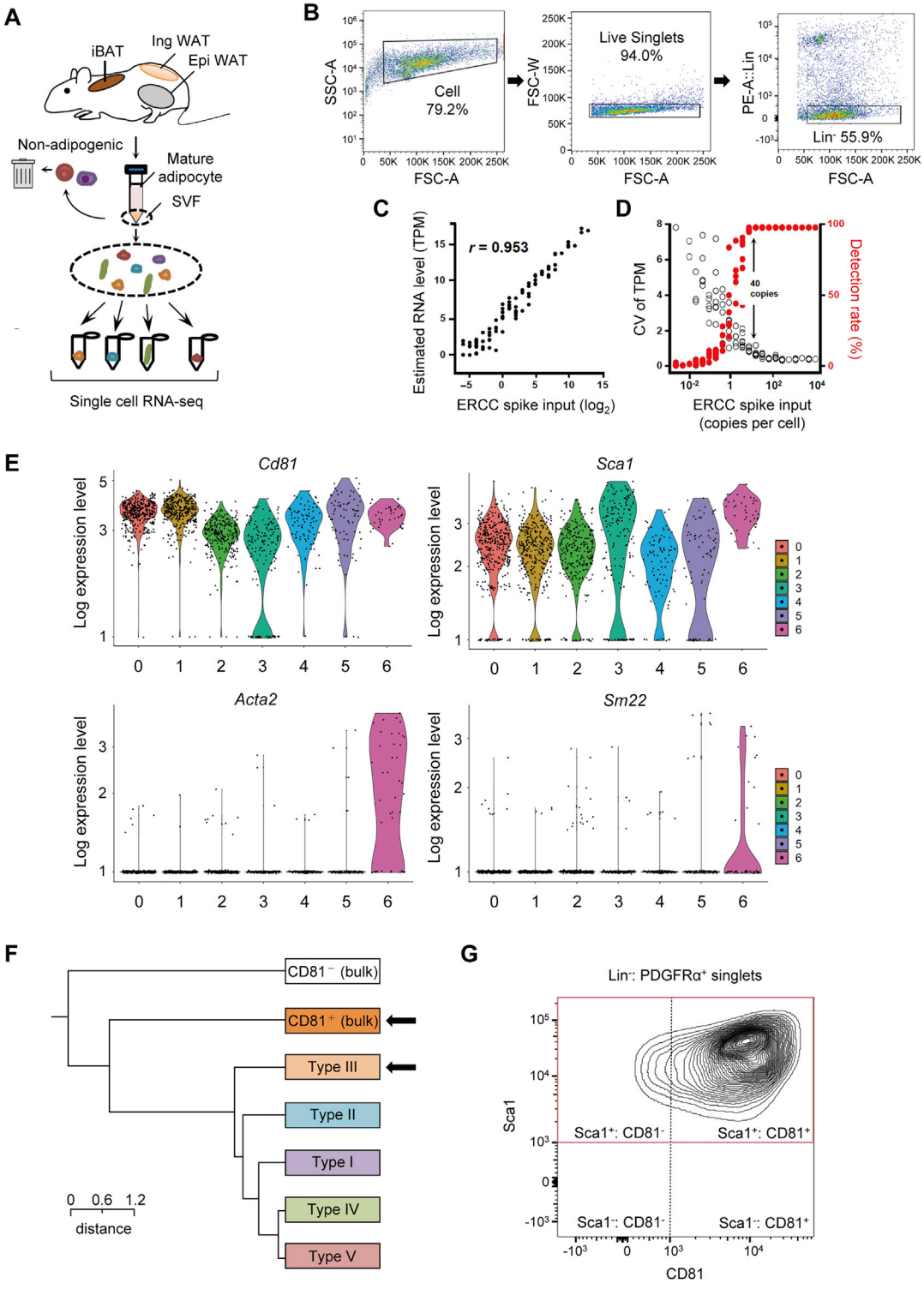

(legend on next page)

Figure S1. Technical Validation of the Single-Cell RNA-Seq Analysis, Related to Figure 1

(A) Illustration of the scRNA-seq experiment. scRNA-seq analysis in lineage$^-$ (Lin$^-$) cells from the stromal vascular fraction (SVF) of mouse adipose tissue.

(B) Sequential gating to isolate Lin$^-$ cells in the SVF from the adipose tissue.

(C) Relationship between estimated RNA level (TPM: transcripts per kilobase million) in single-cell RNA-seq and External RNA Controls Consortium (ERCC) spike input. Note that estimated RNA levels are positively correlated with ERCC spike input (r = 0.953).

(D) Relationship between coefficient of variation (CV) of TPM or detection rate (%) and ERCC spike input (copies per cell).

(E) Meta-analysis of scRNA-seq data GSE111588. Violin plots showing mRNA levels of indicated genes (*Cd81, Sca1, Acta2* and *Sm22*) in type 0 to 6 cell clusters. Note that *Cd81*, *Sca1*, *Acta2*, and *Sm22* are highly enriched in Type 6 cluster.

(F) Hierarchical clustering of bulk CD81$^+$, bulk CD81$^-$ and stromal cell types identified in Figure 1A. The horizontal distance represents similarities among each cluster. See the bulk RNA-seq transcriptomics in Figure 3.

(G) Sca1 and CD81 expression levels in Lin$^-$ PDGFRα^+ cells in the SVF from mouse inguinal WAT. Note that all the Lin$^-$ PDGFRα^+ cells are marked by Sca1 in the SVF from the inguinal WAT.

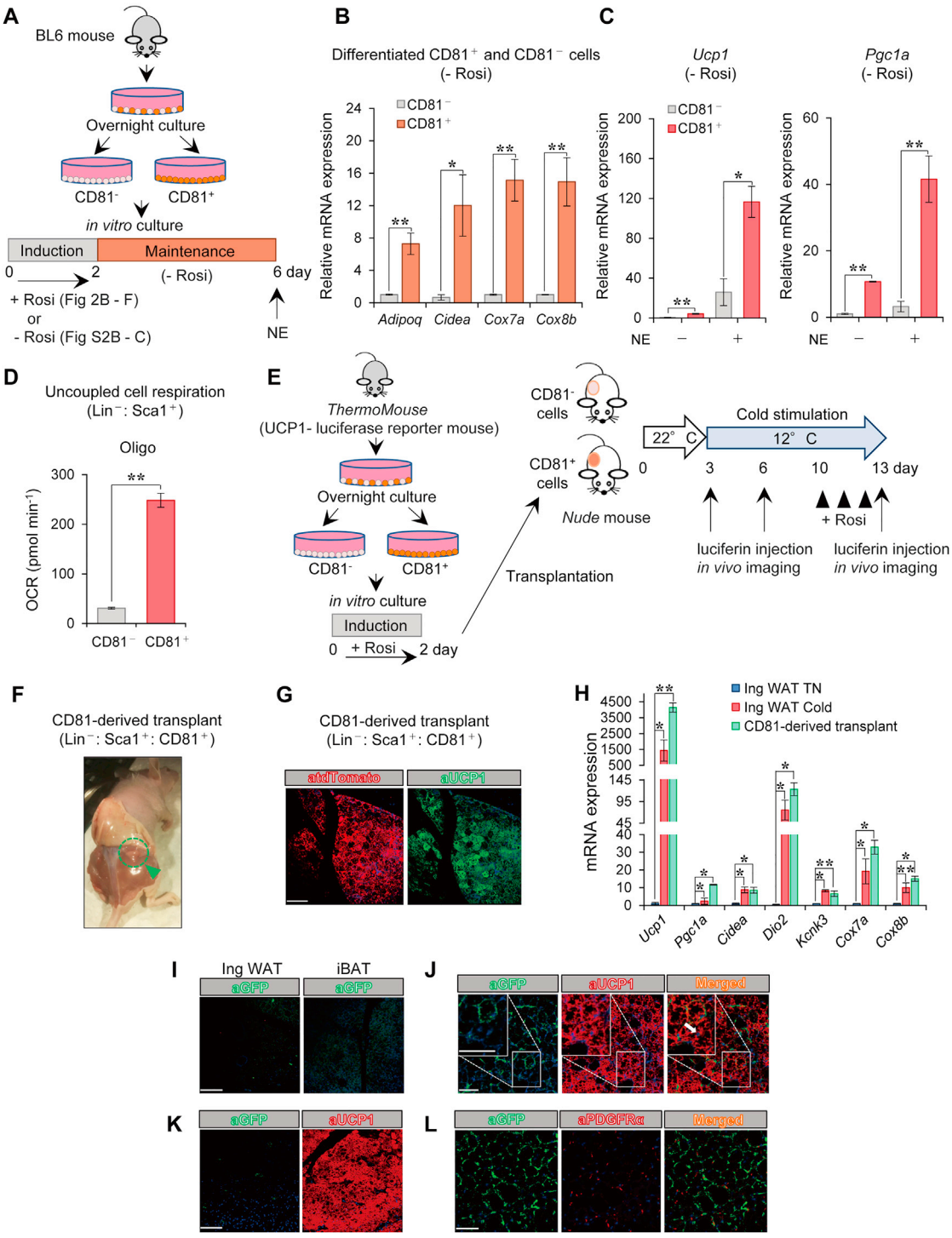

Figure S2. CD81+ Stromal Cells Give Rise to Beige Adipocytes, Related to Figure 2

(A) Schematic illustration of the experiments in culture cell studies. CD81+ cells (Lin-: Sca1+: CD81+) and CD81- cells (Lin-: Sca1+: CD81-) were isolated from the SVFs of Ing WAT of BL6 mice (8-10 weeks of age) after overnight culture. Isolated cells were differentiated for 6 days under an adipogenic condition and stimulated with or without norepinephrine (NE) for 4 hours prior to harvest. During the adipogenic induction phase during day 0 to day 2, cells were cultured with rosiglitazone (Figures 2B–2F) or without rosiglitazone (Figure S2B-C).

(B) Relative mRNA expression of adipogenic and thermogenic genes in differentiated CD81- cells and CD81+ cells. Cells were differentiated for 6 days under an adipogenic condition without rosiglitazone. mRNA expression relative to *Tbp*. n = 3.

(legend continued on next page)

(C) Relative mRNA expression of *Ucp1* and *Pgc1a* in differentiated CD81$^-$ cells and CD81$^+$ cells. Cells were differentiated for 6 days under an adipogenic condition without rosiglitazone and stimulated with or without NE at 10 μM for 4 hours prior to harvest. mRNA expression relative to *Tbp*. n = 3.
(D) Uncoupled OCR (pmol min^{-1}) in differentiated CD81$^-$ cells and CD81$^+$ cells. Differentiated adipocytes were stimulated with NE at 10 μM and subsequently treated with oligomycin (10 μM). 20,000 cells were seeded onto plates. n = 10. (B, C, D) *p < 0.05, **p < 0.01 by unpaired Student's t test.
(E) Illustration of the transplantation experiments. CD81$^-$ cells and CD81$^+$ cells were isolated from Ing WAT of *ThermoMouse* (UCP1-luciferase reporter mice). Cells were differentiated for 2 days under an adipogenic condition with rosiglitazone and transplanted into the subcutaneous region of nude mice. Luciferase activity of transplanted cells were monitored at day 3, 6, and 13 after transplantation. Nude mice were kept at 12°C after 3 days transplantation. Mice were treated with rosiglitazone (10 mg kg body weight^{-1}) twice daily during day 10 to day 12.
(F) Representative images of CD81-derived transplants. Arrowhead indicates a CD81-derived transplant in the subcutaneous region of nude mice.
(G) Immunofluorescent staining for tdTomato and UCP1 in the transplants in (F). DAPI for counterstaining of immunofluorescent staining. Anti-mCherry antibody was used for tdTomato staining. Note that tdTomato is expressed in fat transplants originated from *ThermoMouse* that express a lufierase-tdTomato fusion protein. Scale bar = 100 μm.
(H) Relative mRNA expression of indicated genes in CD81$^+$ APC-derived transplants. Mice were kept at 12°C cold and rosiglitazone treatment for 10 days. Ing WAT of wild-type mice under a thermoneutral condition (TN: 30°C) and cold-acclimated mice at 8°C for 3 days were used as references. mRNA expression relative to *Tbp*. Ing WAT (TN), n = 3; Ing WAT (Cold), n = 5; Transplant, n = 7. *p < 0.05, **p < 0.01 by unpaired Student's t test with Bonferroni's correction.
(I) Unstained signal for GFP in the Ing WAT (left) and interscapular BAT (iBAT; right) of *Cd81*-lineage reporter mice. Scale bar = 100 μm.
(J) Immunofluorescent staining for GFP and UCP1 in the posterior region of Ing WAT of *Cd81*-lineage reporter mice at 8°C. Arrow indicates GFP$^-$ beige adipocytes (GFP$^-$: UCP1$^+$ cells). Scale bar = 50 μm.
(K) Immunofluorescent staining for GFP and UCP1 at 8°C in iBAT of *Cd81*-lineage reporter mice. Scale bar = 100 μm.
(L) Immunofluorescent staining for GFP and PDGFRα in the Ing WAT of *Cd81*-lineage reporter mice at 8°C. Scale bar = 50 μm.
Data in (B, C, D, H) are represented as mean ± SEM.

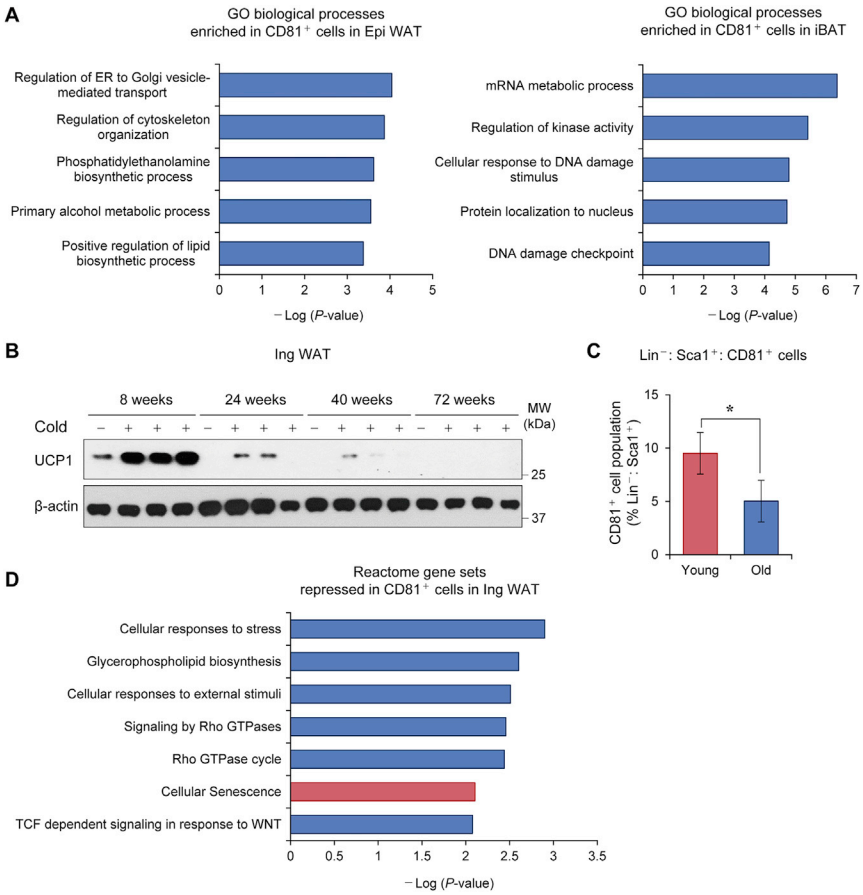

Figure S3. Characterization of CD81$^+$ Cells in Adipose Tissues, Related to Figure 3

(A) The upregulated signaling pathways in CD81$^+$ cells relative to CD81$^-$ cells from Epi WAT, and iBAT of BL6 mice (Top 5 signaling pathway). GO analysis was performed in transcriptomics data of CD81$^+$ cells and CD81$^-$ cells by Metascape. Epi WAT,n = 3; iBAT, n = 2.

(B) Immunoblotting for UCP1 in the Ing WAT of BL6 mice at 8 weeks old, 24 weeks old, 40 weeks old, and 72 weeks old mice. Male BL6 mice were kept at 22°C or 8°C for 5 days. β-actin as a loading control. Molecular weight (MW) is shown on the right.

(C) CD81$^+$ cell population (%) of Lin$^-$: Sca1$^+$ cells in the Ing WAT of young mice (8-10 weeks old) and old mice (60 weeks old). Male BL6 mice were kept at 22°C. Cells were isolated from the SVFs of above mice without overnight culture. n = 12 per group. *p < 0.05 by unpaired Student's t test.

(D) The downregulated signaling pathways in CD81$^+$ cells relative to CD81$^-$ cells from Ing WAT (10 weeks old). Reactome gene sets analysis was performed in transcriptomics data of CD81$^+$ cells and CD81$^-$ cells by Metascape. n = 3.

Data in (C) are represented as mean ± SEM.

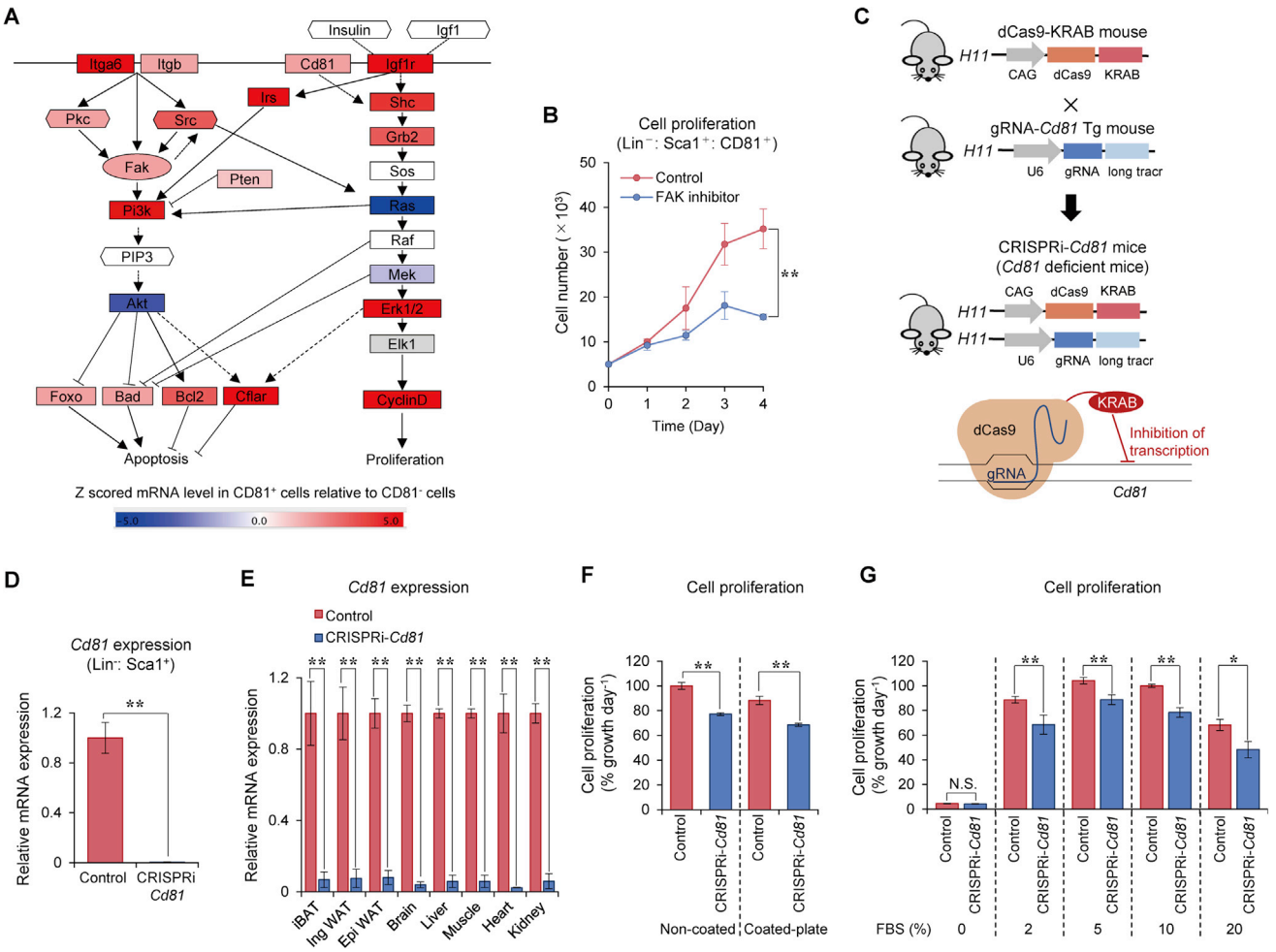

Figure S4. The Requirement of FAK for CD81⁺ APC Proliferation, Related to Figure 4

(A) Gene expressions related to FAK signaling pathway enriched in CD81⁺ cells relative to CD81⁻ cells in the Ing WAT. The color scale shows intensity representing the mRNA levels in blue (low expression)-white-red (high expression) scheme. n = 3.

(B) Time-dependent effect of an ATP competitive FAK inhibitor, PF-573228, on primary CD81⁺ cell growth. Ing WAT-derived CD81⁺ cells were seeded on non-coated plates. Cells were treated with PF-573228 at a dose of 1 μM or vehicle (DMSO) for indicated time. Culture media containing FAK inhibitor or vehicle were replaced every 24 hours. n = 3. **p < 0.01 by two-way repeated-measures ANOVA.

(C) Mice expressing dCas9-KRAB on the H11 locus (dCas9-KRAB mouse) were crossed with transgenic mice expressing gRNA targeting *Cd81* on the H11 locus to generate CRISPRi-*Cd81* mice.

(D) Relative mRNA expression of *Cd81* in Lin⁻: Sca1⁺ stromal cells from Ing WAT of CRISPRi-*Cd81* mice and littermate control mice. mRNA expression relative to *Tbp*. n = 6.

(E) Relative mRNA expression of *Cd81* in indicated tissues of CRISPRi-*Cd81* mice and littermate control mice. mRNA expression relative to *Tbp*. n = 3.

(F) Validation of cell culture conditions to assess APC proliferation. Lin⁻: Sca1⁺ cells from the Ing WAT of CRISPRi-*Cd81* and control mice were cultured on non-coated culture plates or collagen-coated plates. n = 4.

(G) Ing WAT-derived Lin⁻: Sca1⁺ cells from CRISPRi-*Cd81* and control mice were cultured in media with indicated concentrations of FBS. n = 4. (D-G) *p < 0.05, **p < 0.01 by unpaired Student's t test. N.S., not significant.

Data in (B, D-G) are represented as mean ± SEM.

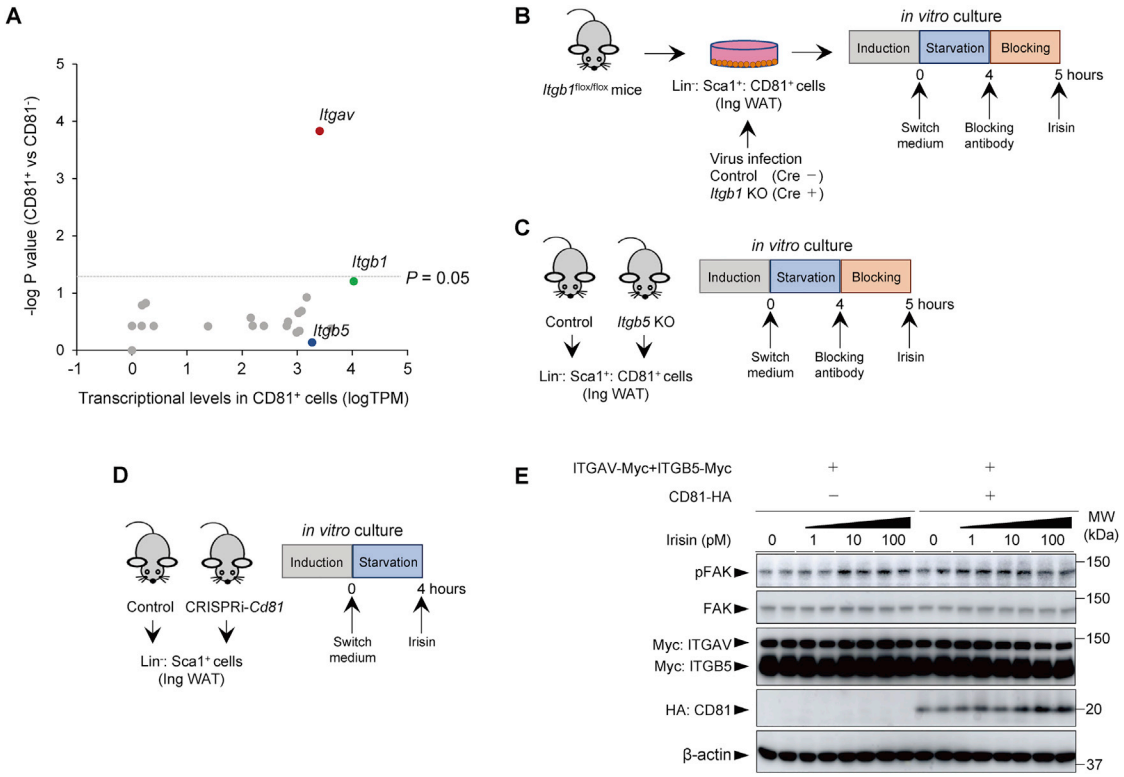

Figure S5. The Requirement of Integrins for CD81-FAK Signaling, Related to Figure 4

(A) Transcriptional profile of integrin family members in CD81$^+$ cells from Ing WAT of BL6 mice (10 weeks old). Isolated cells were analyzed by RNA-sequencing. n = 3.

(B) Illustration of the experiment in Figure 4F. CD81$^+$ cells were isolated from Ing WAT of *Itgb1*$^{flox/flox}$ mice. Cells were infected with retrovirus containing Cre or an empty vector control, followed by hygromycin selection at a dose of 150 μg ml^{-1}. Isolated cells were cultured until confluency and incubated for additional 2 days under adipogenic conditions. Subsequently, cells were cultured in FreeStyle 293 Expression medium for starvation. After 4 hours of starvation, cells were treated with antagonistic antibodies against integrin β1 (ITGB1) or integrin β5 (ITGB5) or mouse IgG control at 5 μg ml^{-1} for 60 min. Subsequently, cells were treated with irisin at 100 pM for 5 min.

(C) Illustration of the experiment in Figure 4H. CD81$^+$ cells were isolated from Ing WAT of *Itgb5* KO mice and wild-type control (129Sv). Cells were cultured and treated with irisin as described in (B).

(D) Illustration of the experiment in Figure 4I. Ing WAT-derived Lin$^-$: Sca1$^+$ cells from CRISPRi-*Cd81* mice and littermate control mice were cultured as described in (B).

(E) Immunoblotting for FAK phosphorylation (pTyr397), total FAK, and β-actin in HEK293T cells expressing integrin αV (ITGAV) and integrin β5 (ITGB5) in the presence or absence of CD81. Cells were subsequently treated with irisin at 1 pM, 10 pM, and 100 pM for 5 min.

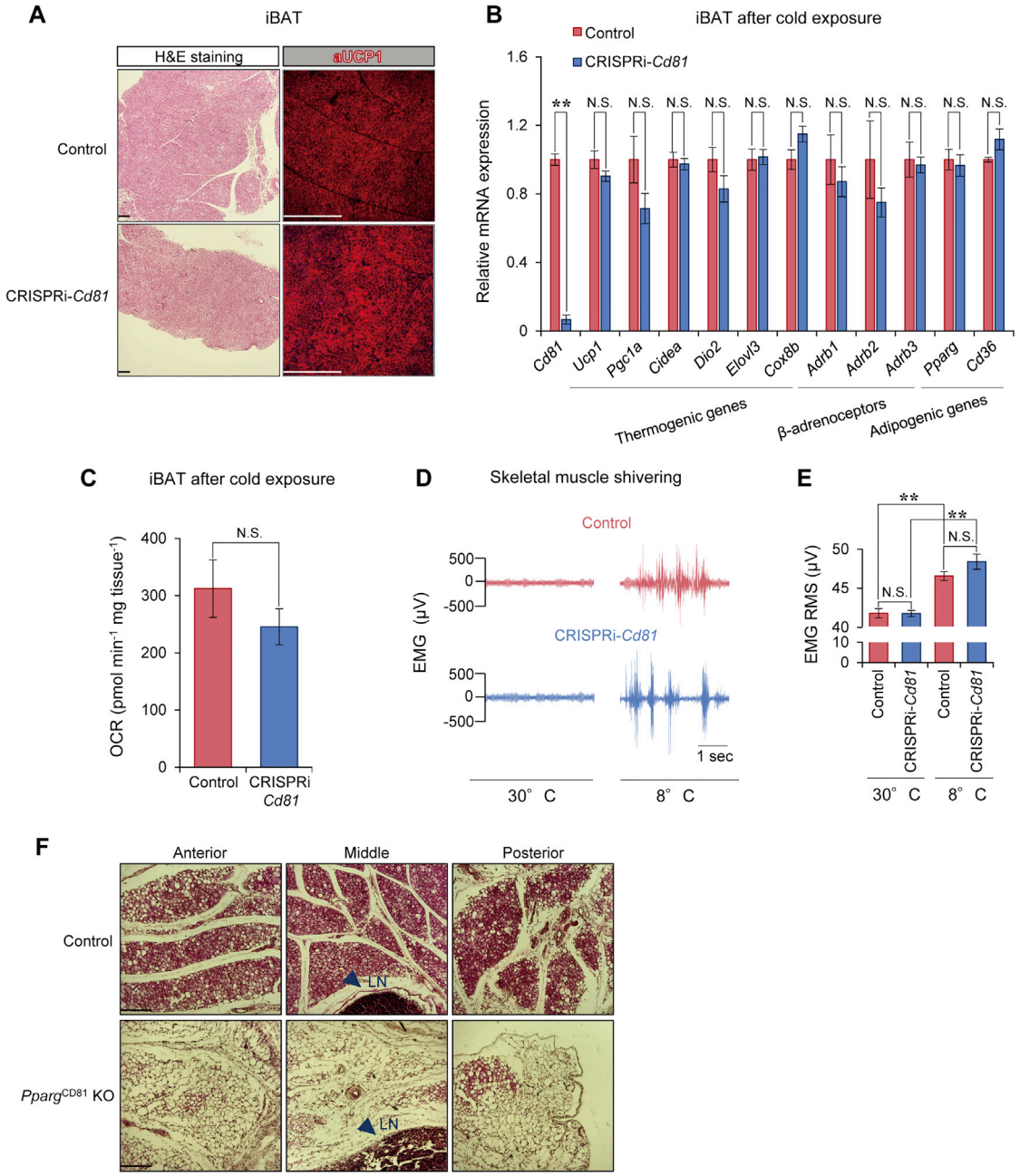

Figure S6. CD81 Is Dispensable for Brown Adipocyte Biogenesis in iBAT and Muscle Shivering, Related to Figure 5

(A) Representative images of H&E staining and UCP1 immunofluorescent staining in iBAT of control mice (top) and CRISPRi-*Cd81* mice (bottom) following cold exposure. Scale bar = 200 μm.

(B) Relative mRNA expression of indicated genes in the iBAT of mice in (A). mRNA expression relative to *Tbp*. n = 5.

(C) OCR in the iBAT of mice after cold exposure. Punch-biopsy tissues (1.0 mg) were analyzed by the Seahorse XF Analyzer. n = 4. (B, C) **p < 0.01 by unpaired Student's t test. N.S., not significant.

(D) Representative electromyography (EMG) traces in skeletal muscle for CRISPRi-*Cd81* mice and control mice at 30°C and 8°C.

(E) Quantification of the images in (D) converted to the root mean square (RMS). n = 3. **p < 0.01 by one-way ANOVA followed by Bonferroni's post hoc test. N.S., not significant.

(F) Representative images of H&E staining in the Ing WAT of *Pparg*^{CD81} KO and control mice after 8°C cold environment for 10 days. Arrowhead indicates lymph node (LN). Scale bar = 200 μm.

Data in (B, C, E) are represented as mean ± SEM.

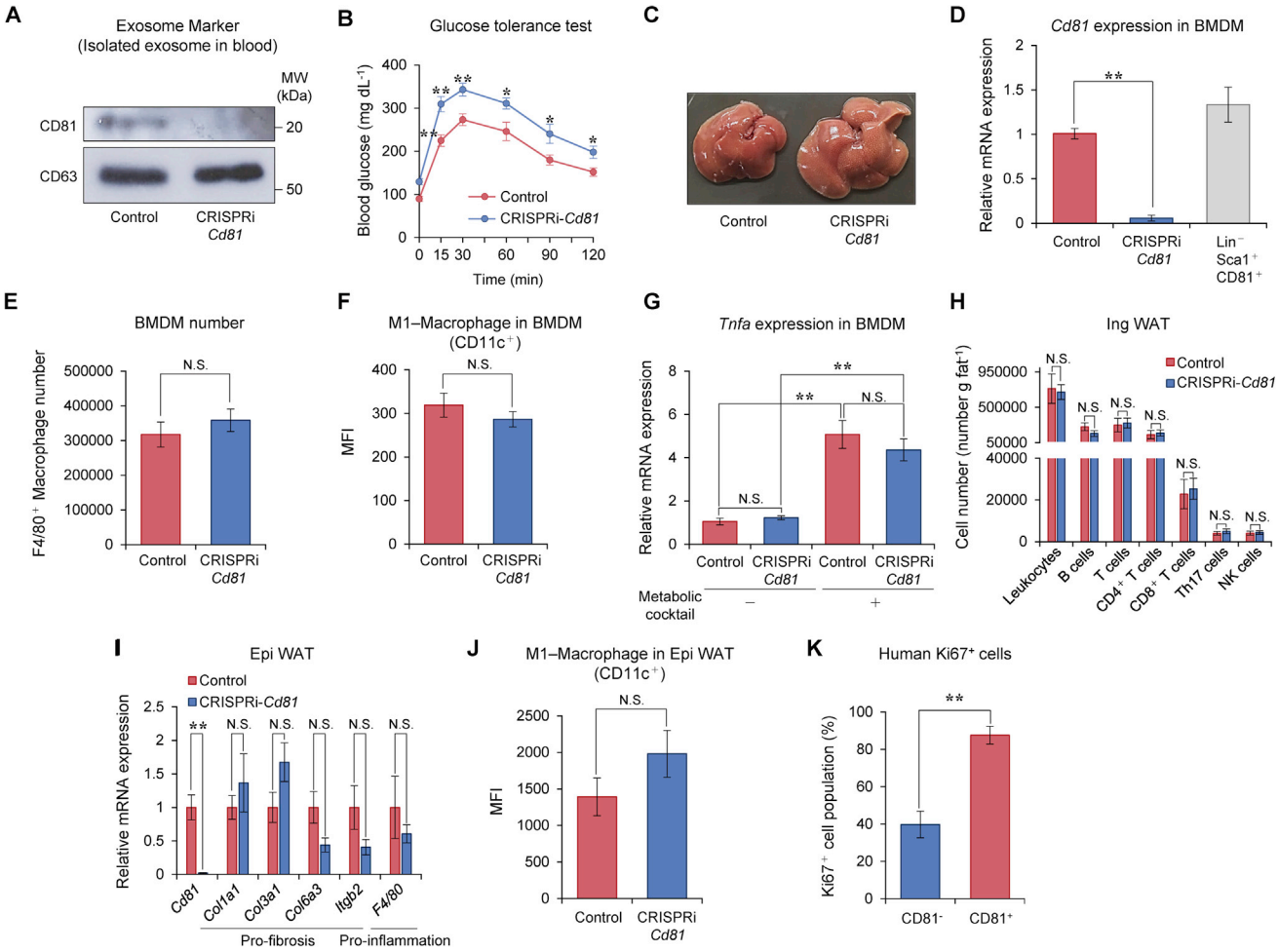

Figure S7. Metabolic Phenotype of CRISPRi-*Cd81* Mice, Related to Figure 6

(A) Immunoblotting for CD81 and exosome marker (CD63) in isolated exosome from the blood of CRISPRi-*Cd81* mice and control mice on HFD for 8 weeks.

(B) GTT in CRISPRi-*Cd81* and control mice on HFD for 2 weeks. Mice were fasted for 6 hours and glucose (1.5 g kg body weight^{-1}) was administered via i.p. Note that body-weight between CRISPRi-*Cd81* mice and littermate controls was indistinguishable at 2 weeks of HFD. Control, n = 8; CRISPRi-*Cd81*, n = 6. *p < 0.05, **p < 0.01 by two-way repeated-measures ANOVA with post hoc test by unpaired Student's t test.

(C) Representative images of the liver of CRISPRi-*Cd81* mice and control mice on 10 weeks of HFD.

(D) Relative mRNA expression of *Cd81* in the BMDM from CRISPRi-*Cd81* mice and control mice, and CD81$^+$ cells in the Ing WAT of BL6 mice. CRISPRi-*Cd81* mice and control mice were on HFD for 10 weeks. mRNA expression relative to *Hprt*. BMDM, n = 6; CD81$^+$ cells, n = 3.

(E) The number of macrophages (F4/80$^+$) in BMDM cultures differentiated from bone marrow of CRISPRi-*Cd81* mice and control mice, quantified by FACS. Mice were on a high-fat diet for 10 weeks. n = 6.

(F) The expression of M1-like macrophage marker (CD11c) among total macrophages (F4/80$^+$) in BMDM cultures from CRISPRi-*Cd81* mice and control mice by FACS (MFI). Mice were on HFD for 10 weeks. n = 6.

(G) Relative mRNA expression of *Tnfa* in the BMDM from CRISPRi-*Cd81* mice and control mice on 10 weeks of HFD. Cells were stimulated with or without metabolic cocktail (30 mM glucose, 10 nM insulin and 0.5 mM palmitic acid) for 18 hours. mRNA expression relative to *Hprt*. n = 6. **p < 0.01 by one-way ANOVA followed by Bonferroni's post hoc test. N.S., not significant.

(H) The absolute number of leukocytes (CD45$^+$), B cells (CD45$^+$: CD3$^-$: CD19$^+$), T cells (CD45$^+$: CD3$^+$), CD4$^+$ T cells (CD45$^+$: CD3$^+$: CD4$^+$), CD8$^+$ T cells (CD45$^+$: CD3$^+$: CD8$^+$), Th17 cells (CD45$^+$: CD3$^+$: CD4$^+$: IL-23R$^+$), and NK cells (CD45$^+$: CD3$^-$: CD4$^-$: CD8$^-$: CD19$^-$: NKp46$^+$) per gram of Ing WAT of CRISPRi-*Cd81* mice and control mice by FACS. Mice were on HFD for 10 weeks. Control, n = 8-9; CRISPRi-*Cd81*, n = 5-6.

(I) Relative mRNA expression of indicated pro-inflammatory and pro-fibrosis genes in Epi WAT of CRISPRi-*Cd81* mice and control mice. Mice were on HFD for 10 weeks. Control, n = 7; CRISPRi-*Cd81*, n = 6. mRNA expression relative to *Tbp*.

(J) The expression (MFI) of M1-like macrophage marker (CD11c) among total macrophages (CD45$^+$: CD64$^+$) in Epi WAT of CRISPRi-*Cd81* mice and control mice on 10 weeks of HFD. Control, n = 9; CRISPRi-*Cd81*, n = 6.

(K) Ki67$^+$ cell population (%) in CD81$^-$ (Lin$^-$: PDGFRα^+: CD81$^-$) and CD81$^+$ cells (Lin$^-$: PDGFRα^+: CD81$^+$) in human subcutaneous WAT biopsies. n = 7. (D-F, H-K) **p < 0.01 by unpaired Student's t test. N.S., not significant.

Data in (B, D-K) are represented as mean ± SEM.